UNIVERSIDADE D
COIMBRA

Gonçalo Moreira Dias

Time-Gated Fluorescence Lifetime Microscope with Light Sheet Illumination

Thesis submitted to the University of Coimbra in fulfillment of the requirements for the Master's Degree in Engineering Physics under the scientific supervision of Ph. D. António Miguel Lino Santos Morgado.

September of 2022

FACULDADE DE CIÊNCIAS E TECNOLOGIA
UNIVERSIDADE D COIMBRA

MASTER'S DEGREE IN ENGINEERING PHYSICS

Time-Gated Fluorescence Lifetime Microscope with Light Sheet Illumination

---

Gonçalo Moreira Dias

Thesis submitted to the
University of Coimbra for the degree of
Master in Engineering Physics

Supervisor:
Prof. Dr. António Miguel Lino Santos Morgado

Coimbra, September of 2022

Agradecimentos

Ao Professor Doutor Miguel Morgado, agradeço toda a sua ajuda, compreensão e disponibilidade que me levaram a completar este projeto. O meu muito obrigado, Professor. À Doutora Ana Batista, pela ajuda e disponibilidade que sempre teve comigo.

À minha família. Aos meus pais, Sónia e Edgar, ao Miguel e aos meus irmãos, Vicente e Mateus, pela educação, paciência, esforço e motivação. Aos responsáveis de ser quem sou e estar onde estou. Não estaria certamente aqui sem cada um de vocês.

Aos meus amigos. Ao João e ao Leandro, irmãos que não são de sangue. À Rita Rouxinol, pela amizade única e genuína. Seremos sempre "unha e carne". Ao Manuel e à Mária, pelo orgulho que são para mim. À Inês, ao Rodrigo, ao Diogo e ao Zé, por todos os momentos que partilhámos. À Rita Barradas, pelo orgulho, ligação e pela crença que sempre teve em mim. Um agradecimento especial ao Jorge, o meu companheiro desde o início desta aventura. Por todos os desafios que já superámos juntos, pela amizade e lealdade.

Aos que me acompanharam no Polo Aquático da AAC, na Physis e na Pollux. O meu percurso académico de nada serviria sem os momentos que vivi com vocês.

Por último ao meu avô Virgílio. Serás para sempre a minha referência e pilar. Pelos valores que me incutiste e que tenho enraizados em mim. Prometo não parar de te orgulhar.

A todos, o meu muito obrigado!

Abstract

Optical imaging technologies can assess the metabolic activity of biological tissues. This study focus on developing a system capable of studying thick ocular tissues, like corneas. The system was based on non-invasive fluorescence lifetime imaging microscopy techniques. These techniques may help detect dysfunction and prevent disorders from developing into irreversible states.

In order to image fluorescence between 520 and 570 nm in thick biological tissues, this project focused on the development of a Time-Gated fluorescence lifetime microscope with light-sheet illumination at 440 nm.

The microscope was characterized through testing of its optical and timing properties. The system has an axial resolution of around 8.6 μm. This result represents an improvement between 14 to 42% over what was initially required. The measured fluorescence lifetime has a relative accuracy error that ranges from 3 to 13%, depending on the used gate width.

Animal corneas and induced fluorescent onion cells were imaged to test the microscope. The results obtained did not fulfill the main objective of this project.

Except for the optical sectioning performance, the acquired values satisfied the system requirements. The implemented microscope, however, performs as expected and enables assessment of its use for imaging biological tissues. In order to image thick tissues with good contrast, the microscope must be modified to further decrease the light-sheet thickness, which helps to improve the optical sectioning.

Keywords: Time-Gated, Fluorescence lifetime imaging microscopy, Light-sheet, Corneas, Flavin Adenine Dinucleotide

Resumo

As tecnologias de imagiologia ótica são ferramentas que permitem avaliar a atividade metabólica de tecidos biológicos. Este estudo foca-se no desenvolvimento de um sitema capaz de adquirir imagens de tecidos oculares espessos como, por exemplo, cóneas. O sistema é baseado em técnicas microscopia de tempo de vida de fluorescência. Estas técnicas poderão ajudar a detetar disfunções e previnir que distúrbios possam progredir para estados irreversíveis.

De modo a adquirir imagens de fluorescência entre 520 e 570 nm em tecidos biológicos espessos, este projecto focou-se no desenvolvimento de a um microscópio de tempo de vida de fluorescência com iluminação light-sheet a 440 nm.

O microscópio foi caracterizado com recurso a testes que avaliaram as suas propriedades ópticas e de temporização. O sistema tem uma resolução axial de cerca de 8,6 μm. Este resultado representa uma melhoria entre 14 a 42% relativamente ao que era inicialmente requerido. O tempo de vida de fluorescência medido, tem um erro relativo de exactidão que varia de 3 a 13%.

Foram utilizadas córneas de animais e células de cebola com fluorescencia induzida para testar o microscópio. Os resultados obtidos não cumprem o objetivo principal deste projeto.

Constata-se que, excetuando o desempenho do seccionamento óptico, os valores medidos satisfazem com os requisitos do sistema. Para obtenção de imagens de tecidos espessos com bom contraste, o microscópio deve ser melhorado para diminuir ainda mais a espessura da light-sheet e melhorar o seccionamento óptico.

Palavras-chave: Time-Gated, Microscopia de tempo de vida de fluorescência, Light-sheet, Córneas, Flavin Adenine Dinucleotide

Contents

List of Figures

List of Tables

1

Introduction

1.1 Objectives

This work aims to re-design and implement a Time-Gated fluorescence lifetime microscope with light-sheet illumination to image thick biological tissues. Hence, the work was divided into three phases. The first phase involves re-designing and modifying the microscope setup used in the previous study [1]. The second stage is the microscope's test and characterization to estimate the image and the lifetime determination quality. The third and last phase consists of ex vivo tests, in this case, corneas.

The system's design had to be slightly changed some months before the end of this study due to limitations of the microscope detection objectives. These objectives provided a 20x and 40x magnification. However, the working distance was very short and incompatible with this study's objectives due to the proximity between the sample and the objective. The incorporation of a new objective solved this problem.

1.2 Context and motivation

This study occurs in the context of research projects carried out at Coimbra Institute for Biomedical Imaging and Translational Research's Instrumentation Group (CIBIT). One of the primary goals of this group is to investigate and develop optical imaging technologies for imaging and evaluating the metabolism of biological tissues, particularly ocular tissues.

The thin transparent tissue in front of the eye is the cornea. It is a highly differentiated tissue with particular properties to preserve transparency and withstand harmful external elements, including dehydration, microbial invasion, and trauma. It also allows for the refraction and transmission of light. This tissue is responsible for

about 70% of the total refractive power of the eye [3, 4]. Corneal pathologies are the second major cause of blindness worldwide. These pathologies can affect vision, cause pain, and even lead to blindness. For example, in some African areas, 90% of blindness is from corneal pathology [5]. Thus, a non-invasive early detection technique that may detect dysfunction and avoid disorders from developing into irreversible states may be of therapeutic importance.

Structural imaging is the most common method of clinical imaging of the cornea. However, this method is not able to identify the cellular abnormalities that are involved in the development of the disease. Therefore, a functional imaging method should be developed to fulfill this goal.

This work followed a previous project with the same aim [1]. Unfortunately, the results obtained with the previous system lack good optical sectioning and working distance. During this project, two new objectives were bought. Therefore, it was reasonable to anticipate an improvement in the performance of the system.

1.3 Requirements analysis

System requirements can be divided into functional and non-functional. The functional requirement is that it must be possible to obtain lifetime fluorescence images in thick, low scattering biological tissues, with a thickness of less than 500 μm, for excitation at 440 nm.
The system's non-functional requirements are presented in table 1.1.

Table 1.1: Non-functional requirements.

Parameter	Value
Optical sectioning	15-20 μm
Temporal resolution	300-400 ps
Lateral resolution	20 μm
Field of view	200x300 μm
Accuracy error on the lifetime	$< 10\%$
Precision error on the lifetime	$< 10\%$

1.4 Thesis content

This thesis is divided into six chapters. This first chapter holds the objectives and context of this work. In addition, it includes the context and motivation for doing

this project and the critical requirements the system must achieve.

The second chapter describes the principles of the fluorescence process, Fluorescence Lifetime Imaging Microscopy (FLIM), light-sheet illumination, and the standard technologies used to measure fluorescence lifetime. This chapter also includes some historical context and evolution over the years.

The third chapter presents the microscope implementation. It contains a description of each component and module of the microscope, including their function and specifications.

The fourth chapter addresses the microscope evaluation. It contains the evaluation of the field of view and lateral, axial, and temporal resolutions.

The fifth chapter contains the results of all imaging experiments done in this study.

The last chapter includes the discussion and critical review of the results and indications for future work.

2

State of Art

This chapter describes principles of the fluorescence process, FLIM, light-sheet illumination, and the standard technologies used to measure fluorescence lifetime. It also describes some techniques and technologies addressed in this dissertation.

2.1 Fluorescence Lifetime Imaging Microscopy

FLIM is a technique that sits on the fluorescence spectroscopy and microscopy principle. This technique introduced the capability of imaging fluorophores spatial distribution based on the fluorescence lifetime (τ) [6]. Therefore, knowing how the fluorescence process occurs and studying a sample decay process is essential to better understand this technique.

2.1.1 Fluorescence

The first fluorescence lifetime measurements took place around 1920 [7]. Fluorescence is the emission of light within nanoseconds after absorbing light of a shorter wavelength. The average time the molecule remains in its excited state before returning to the ground state is fluorescence lifetime (τ). This process occurs in fluorophores, molecules, such as proteins, organic compounds, or polymers. These molecules absorb light of specific wavelengths and, subsequently, emit light at longer wavelengths [8, 9].

FLIM is an imaging technique capable of showing molecular contrast based on fluorescence lifetime information. Furthermore, the detected information shows the intensity of the signal and helps estimate intrinsic properties of the fluorophores and their microenvironment [10, 11, 8, 9].

The Jablonski diagrams are typically simple illustrations of the processes between absorption and emission of light by a molecule. For example, the diagram shown in

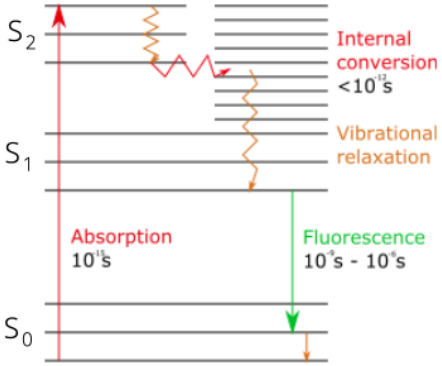

Figure 2.1: Jablonski diagram based on [11, 12].

figure 2.1 is one of the many diagrams used to represent diverse molecular processes that occur in excited states. This diagram shows the singlet second, first, and ground electronic energy states represented by S_2, S_1 and S_0, respectively. The vertical lines between the vibrational energy levels represent the absorption (red) and fluorescence (green) characteristic transitions between states.

After the absorption of one photon, the molecule can be excited to a given vibrational level of the higher energy singlet states (S_1 or S_2), depending on the energy of the photon, given by:

$$E = \frac{hc}{\lambda} \tag{2.1}$$

where h is the Plank constant, c is the speed of light, and λ is the wavelength. The minimum energy to cause the fluorescence effect is the one that takes an electron from S_0 to S_1. The absorption transition is a fast process (femtoseconds) [11, 7, 9].

After absorption, part of the energy dissipates by internal conversion and vibrational relaxation, leaving the molecule in the lowest vibrational state of the electronic state S_1. These processes occur within or even less than 10^{-12}s. Therefore, the fluorescence process is a consequence of a thermally equilibrated excited state [11, 9]. Returning to the ground state happens either by a non-radiative or a radiative decay. This radiative decay is called fluorescence. The thermal equilibrium is then rapidly reached, typically within 10^{-12}s. The difference between the absorption and emission wavelengths is called the Stokes shift [11].

As mentioned, the fluorescence lifetime (τ) is an intrinsic parameter of a fluorophore molecule, although it can be modified by conditions of the fluorophore's micro-environment. Equation 2.2 shows how it is defined with k_r and $k_n r$ being the

radiative and non-radiative rate constants [13, 11].

$$\tau = \frac{1}{k_r + k_{nr}} \tag{2.2}$$

We can also assess the efficiency of the fluorescence process by measuring the quantum yield, given by equation 2.3 (Φ). Quantum yield is the ratio between emitted photons and absorbed photons [13, 11].

$$\Phi = \frac{k_r}{k_r + k_{nr}} \tag{2.3}$$

Fluorescence intensity decay curves of fluorophores express themselves by electron depopulation of excited states. For example, suppose N is the number of fluorophores in the excited state S_1. In that case, dN is the number of excited fluorophores returning to ground level in the instant dt. Equation 2.4 shows that relation [7].

$$dN = (k_r + k_{nr})N(t)dt \tag{2.4}$$

Where N(t) is given by:

$$N(t) = N_0 e^{\frac{-t}{\tau}} \tag{2.5}$$

The intensity decay function, I(t), is obtained it by integrating equation 2.4 and also considering equation 2.2. It is assumed that the intensity I_0 is proportional to the number of excited fluorophores, N_0, at t = 0 after the excitation pulse [13, 1, 10]. So, the fluorescence intensity decay is given by equation 2.6.

$$I(t) = I_0 e^{\frac{-t}{\tau}} \tag{2.6}$$

When considering more than one fluorophore, we may describe the fluorescence decay with a multi-exponential form. The equation 2.7 represents the fluorescence decay of the sample with several fluorophores with different lifetimes and intensities at t=0 [1].

$$I(t) = \sum_{N}^{i=1} I_i e^{\frac{-t}{\tau_i}} \tag{2.7}$$

2.2 FLIM acquisition techniques

FLIM has two standard options for acquiring the emission signal: frequency domain and time domain. The most significant difference between these two techniques is how the time-resolved fluorescence data are acquired [6, 14]. Figure 2.2 shows how these two acquisition techniques work.

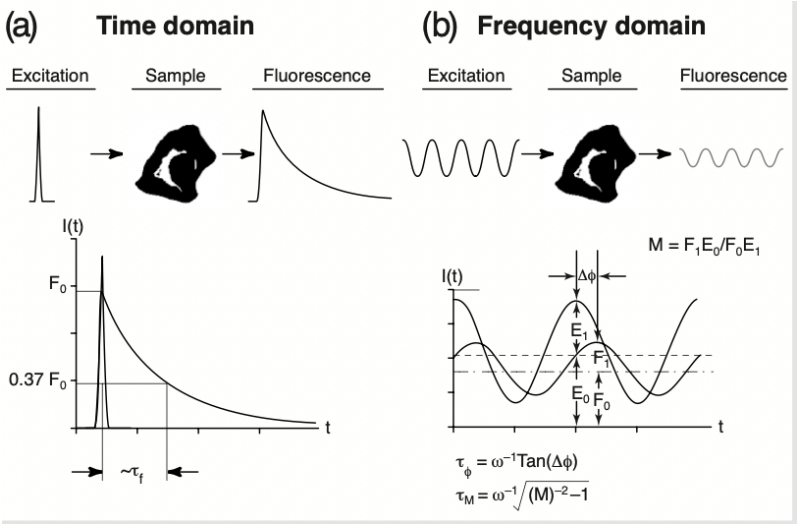

Figure 2.2: Visual representation of time domain (a), frequency domain (b) and the respective output fluorescence signal [15].

The frequency domain uses a sinusoidal intensity-modulated excitation light, as shown in figure 2.2, and gain-modulated detectors. In this technique, the fluorescence emission shows a phase shift and a decrease in modulation due to the delayed fluorescence decay [6, 14, 7].

The time domain uses pulsed excitation sources and time-correlated or time-gated detection. With this technique, after the pulse of excitation, the emitted fluorescence is measured using a time-resolved technique, resulting in decay curves like the ones we can see in figure 2.2 [6, 7].

The most standard time-domain measurement for time-correlated detection is time-correlated single-photon counting (TCSPC). On the other side, the other standard detection technique is time-gated. Time-domain measurements were only possible roughly 40 years later than frequency-domain because of the need for pulsed excitation sources [6, 10, 7].

According to statistical tests, there is an excellent correlation between the lifetimes estimated by the time-domain and frequency-domain fluorometry [14].

2.2.1 Time-Correlated Single Photon Counting technique

Time-Correlated Single Photon Counting technique (TCSPC) uses a detector, followed by a timing discriminator and a time-to-digital converter (TDC) [16, 17]. A laser pulse is sent to a given sample, and the acquisition process is based on timing only the first detected photon. Then, the excitation pulse is timed by a second photodetector or through an electrical synchronization signal provided by the laser. This way, the system measures the time interval between the excitation and the detection of the first fluorescence photon [16, 13, 18].

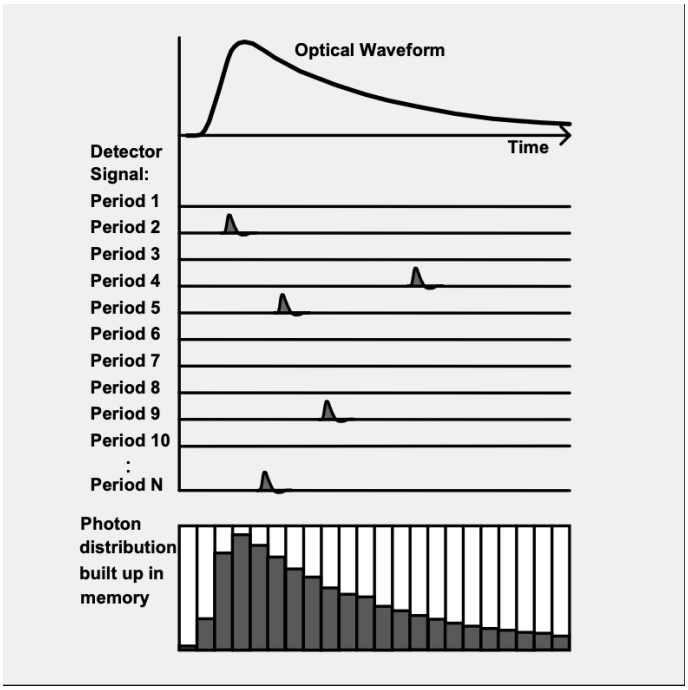

Figure 2.3: Time-Correlated Single Photon Counting technique example [16].

In the TCSPC technique, the light intensity is very low, which means the probability of detecting one photon in one signal period is quite rare. Therefore, it is not necessary to provide the possibility of detecting several photons in one signal period. So, when a photon is detected, the time of the corresponding detector pulse in the signal period is measured [16, 19].

The final result of all the detected photons in many period acquisitions is of the arrival times of the first fluorescence photon, like the one shown in figure 2.3, which, in an ideal system, corresponds to the fluorescence decay curve of the sample. TCSPC has the advantages of recording light signals with high timing resolution and efficiency. The ratio of recorded and detected photons is roughly one. [16, 18].

2.2.2 Time gated

A usual time domain FLIM acquisition method is the time gated (TG) technique. TG consists in accumulating intensity images at specific time windows, called gates. Unlike TCSPC, this technique collects the fluorescence signal while the time gates are opened. This gates are delayed relative to the laser excitation pulse. We can then measure the fluorescence lifetime with the information on the number of photons collected in, at least, two windows [20].

TG technique performance depends on the detection method. Typically TG uses a Gated Optical Intensifier (GOI). This consists of a photocathode, a Microchannel Plate Detector (MCP), and a detection system. As a fluorescence photon reaches the photocathode, an electron is generated and heads to one of the MCP channels. In the MCP channel, that electron will generate, by ionization, several secondary electrons until they all reach the end of the channel, hitting the detection system. The number of times the electron is multiplied depends on the voltage gradient applied to the MCP. When the electrons hit the detection system, typically a phosphor screen, they generate photons. So, the GOI amplifies the number of photons that will reach the imaging device (CCD camera). This is a crucial process due to the usually small intensity of fluorescence signals [20, 10, 21].

The gate control is done by the voltage applied to the photocathode. This voltage is set by a gate pulse that also defines the gate width. This width corresponds to the interval during which the photoelectrons generated at the photocathode of the GOI are able to reach the MCP and, therefore, be multiplied. The gate width is the main contribution to the system's temporal resolution [20].

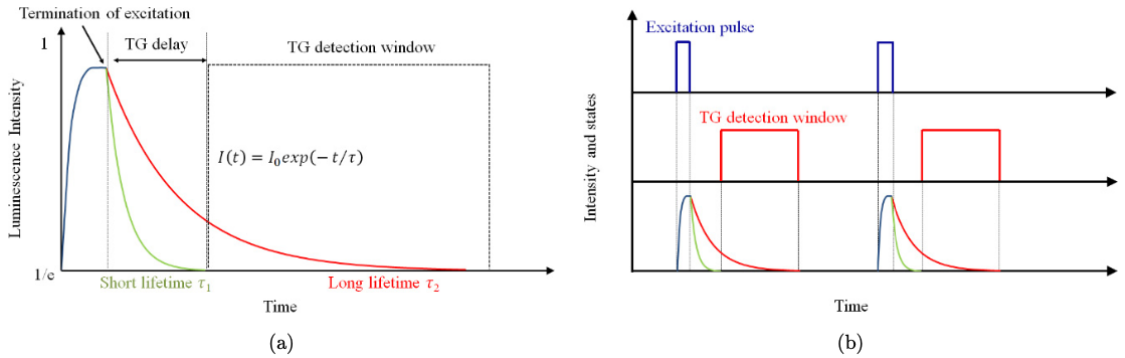

Figure 2.4: Time gated signal acquisition for: (a) a single fluorescence decay; (b) multiple cycles of fluorescence decay [10].

Figure 2.4 shows time gated acquisitions for single exponential decays. In order to determine fluorescence lifetimes of single-exponential decays, two gates are enough.

However, for multiexponential decays, we need more than two time gates. This demands a more complex analysis and longer acquisition time [20].

Compared to TCSPC, the TG technique is less accurate and has a lower time resolution. However, it has shorter electronic dead times and faster acquisition times [10, 20].

2.3 FLIM imaging techniques

There are different techniques to do the imaging process in FLIM images. We can group them by their illumination method: with and without scanning. The most popular technique in scanning optics is confocal microscopy; on the other side, wide-field microscopy does not need scanning illumination [6].

For many years, before confocal microscopy and other scanning methods were available, wide-field microscopy was the only way to perform microscopy. As the name suggests, the entire sample is exposed simultaneously to the light source. The image is created directly on the lens, which then projects it on a camera for digital acquisition. The camera must have the capability of being time-resolved. If the light source is a laser, the setup needs to expand the beam to illuminate the entire sample. Despite being a simple fluorescence imaging technique, it does not have optical sectioning to image thick samples [6, 22].

Confocal fluorescence microscopy is the most popular technique to obtain three-dimensional data sets [22]. It uses a pinhole in the image plane that rejects the signal from out-of-focus regions. As a result, this technique improves axial and lateral resolution. The illumination setup, based on a pulsed or modulated laser source, only illuminates one point at a time. The entire sample is then scanned [6, 22, 18].

2.4 Light-Sheet Fluorescence Microscopy

Light-Sheet Fluorescence Microscopy (LSFM) is an imaging technique based on the illumination of a sample by a laser beam shaped by a cylindrical lens. The beam passes through an illumination objective and forms the light sheet, as shown in figure 2.5. In addition, this method allows scanning the sample along several illumination planes, which are then imaged perpendicularly by the detection objective, and acquired by the camera [23].

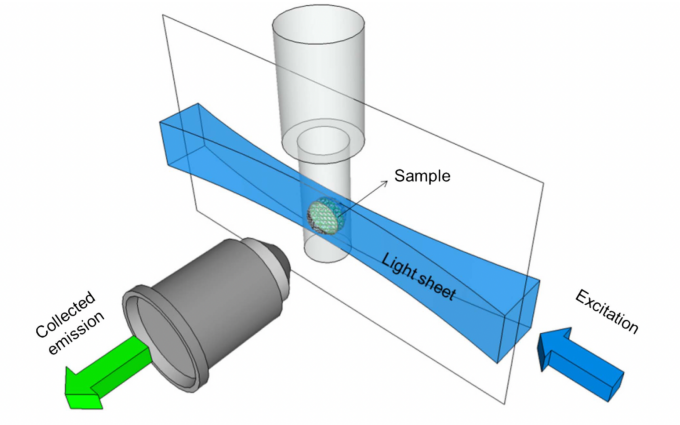

Figure 2.5: LSFM excitation and acquisition. Excitation with the thin optical slice is perpendicular to the detection [24].

The great benefit of this technique is creating a thin plane of light that provides an optical section that only illuminates the area of interest, leading to the excitation of fluorophores only inside the optical section. This characteristic provides optical sectioning [25, 23].

Comparatively to wide-field and confocal microscopy, there is no need to use a beam splitter to separate the illumination, and detection light [22]. As a result, LSFM shows good contrast, fast (2D) high-resolution imaging, and better penetration depth than wide-field and confocal microscopy. Moreover, due to optical sectioning, photobleaching and phototoxicity are also reduced [23, 26].

Light-sheet illumination can be separated into two categories. One is DSLM (Digital Scanned Laser Light-Sheet Fluorescence Microscopy), where a focused beam is quickly moved to the focal plane of the detection lens, resulting in a virtual light sheet. The other is SPIM (Selective-Plane Illumination Microscopy). This technique uses a cylindrical lens to focus the excitation light, resulting in a static light sheet [24].

2.5 Fluorescence lifetime determination

2.5.1 Impulse Response Function

The IRF (Impulse Response Function) is commonly defined as the system response to a Dirac delta function. As FLIM instruments are linear, time-invariant systems, the acquired data corresponds to the convolution of the actual fluorescence decay curve with the IRF of the instrument [13].

The IRF can be measured using non-fluorescent scattering samples or using a known fluorophore with an ultrashort lifetime [13, 27].

2.5.2 FLIMfit

FLIMfit is open-source software that fits the fluorescence decay data for a time-domain system. It uses global analysis to simultaneously fit the decay data of all pixels in the dataset to a multi-exponential model. It assumes the lifetime components are invariant across the dataset. The goodness of the fit is evaluated by the chi-square (χ^2) value and other statistical tests. This open-source software can work with large data sets [28].

This software used the Rapid Global Fitting Method, a method based on a different interpretation of least-squares deconvolution, opening the possibility of fitting large datasets. It also considers parameters like stray light and scattered excitation light, which can influence fluorescence decay [13].

2.5.3 Rapid Lifetime Determination

As mentioned before, one of the standard algorithms to determine fluorescence lifetime is rapid lifetime determination (RLD). With the RLD method, the decay parameters are determined from two (single-exponential decay) or four (double-exponential decay) images, acquired during time gates of equal width, instead of taking multiple images to sample finely the decay curve [29, 13, 30].

The single-exponential decay, I(t), can be calculated using the values of two images, I0 and I1, acquired at two contiguous gates, of width Δt, located over the decay curve [29, 13].

The equation 2.8 gives the fluorescence intensity decay curve, I(t), for a sample with a single fluorescence lifetime, with a pre-exponential factor k. The fluorescence lifetime, τ, is determined using equation 2.9 where I_0 and I_1 are the numerical arrays corresponding to the two acquired images, and Δ t is the gate width. The pre-exponential factor k is given by equation 2.10 [13, 29, 30].

$$I(t) = k \cdot \exp\left(-\frac{t}{\tau}\right) \tag{2.8}$$

$$\tau = \frac{-\Delta t}{ln\left(\frac{I_0}{I_1}\right)} \tag{2.9}$$

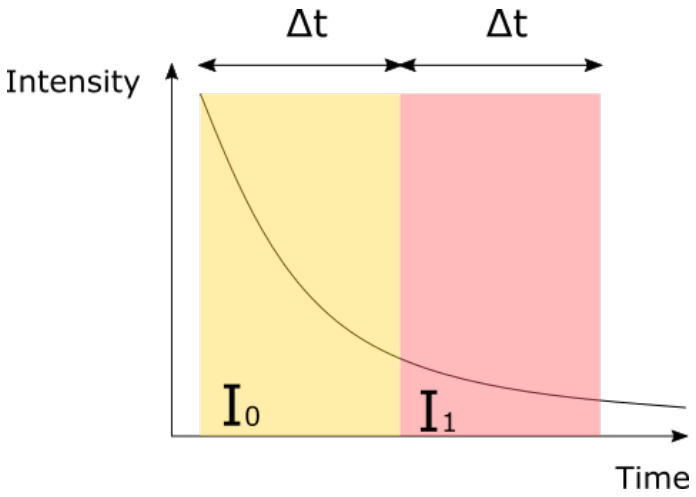

Figure 2.6: Rapid lifetime determination acquisition for a single-exponential decay, based on [13].

$$k = \frac{I_0}{\left(\tau\left(1 - \frac{I_1}{I_0}\right)\right)} \tag{2.10}$$

3

Microscope implementation

As the first chapter tells, this study seeks to measure the fluorescence lifetimes and image biological tissues with a thickness inferior to 500 μm, like corneas tissues, through fluorescence lifetime imaging. To achieve this goal, we implemented a Time-Gated FLIM instrument. The illumination is done perpendicularly to the detection axis by a Light-sheet technique. This illumination technique provides suitable optical sectioning.

Eye corneas contain Flavin Adenine Dinucleotide (FAD) molecules, which, if well measured, can help to indicate anomalies in the metabolic state of corneal cells [13, 31, 32, 33].

The wavelength intervals are crucial to a successful acquisition, being one of the most critical parameters to have in account when designing a system of this complexity. For FAD, the typical excitation goes between 420 and 500 nm, and the emission between 520 and 570 nm [34].

The previous implementation of this system lacked physical stability and needed changes in optical components [1]. For this reason, the first step was redesigning the system. First, a clear one-direction illumination path was created, removing mirrors and unstable elements. Next, the components were placed in just one solid aluminum optical breadboard instead of multiple different-sized boards of the previous study [1]. This way, all the elements are attached to the same board, and the stability problem is solved.

Lastly, two identical new objectives, more suitable for the system requirements, were achieved. These objectives replaced the previous ones providing a considerable increase in working distance (WD) and a better matching to the wavelength range.

The block diagram of the complete setup of the Time-Gated fluorescence lifetime microscope with light-sheet illumination is shown in Figure 3.1. This diagram includes all the system and optical elements of the system. It also gives a representation

of the connection between them.

At the end of the chapter, Figures, 3.16a and 3.16b ,show the new instrument setup.

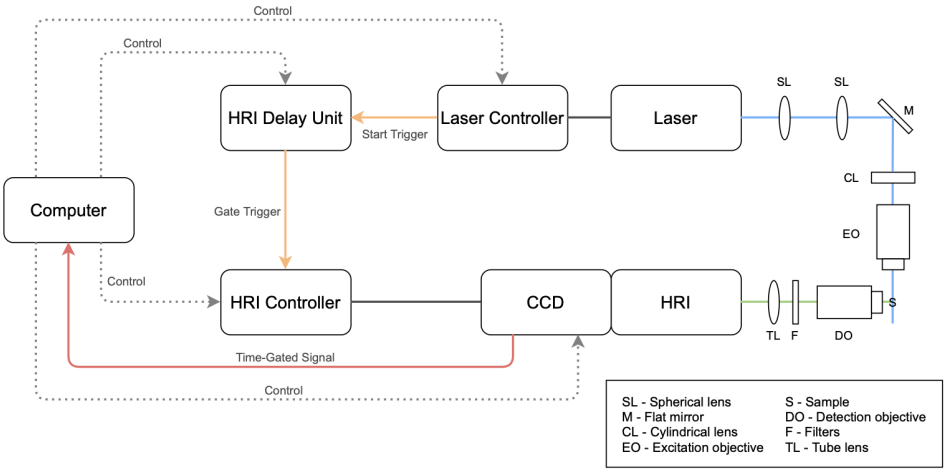

Figure 3.1: Diagram of the complete setup extracted from [1].

3.1 Microscope main units

Several requirements need to be met, from lighting to the ability to acquire the time-gated technique. A pulsed diode laser with a central wavelength of 440 nm ensures that the system can excite the sample. This laser module also sends a trigger signal for every pulse, giving the needed input to an HRI (High Rate Imager) delay module. The generated delay is controlled via the computer. After the delay ends, a GOI (Gate optical imaging) HRI is responsible for creating the gate signals that allow the acquisition of fluorescence photons by a gated-intensified CCD camera. For fluorescence lifetime analysis, it was used the FLIMfit software.

3.1.1 Laser source

The microscope light source is a pulsed diode laser. This laser system is composed of a laser head (PicoQuant LDH-P-C-440M, Berlin, Germany) and a multichannel picosecond driver(PicoQuant PDL 828 “Sepia II”), Figures 3.2a and 3.2b, respectively. The laser’s main specifications are presented in table 3.1.

The laser driver is also responsible for sending the trigger signal to the delay generator. This trigger coincides with each laser pulse.

The laser parameters are adjustable through a computer interface, via USB [35].

(a) **(b)**

Figure 3.2: Diode laser setup from PicoQuant. LDH-P-C-440M laser head and PDL 828 "Sepia II" multichannel controller, (a) and (b), respectively.

Table 3.1: Specifications of the pulsed diode laser [35].

Pulsed diode laser	
Central wavelength (± 10) (nm)	440
Maximum Mean Laser Power (mW)	22.50
Maximum Pulse Repetition rate (MHz)	40
Minimum pulse Width (FWHM) (ps)	63
Maximum pulse Width (FWHM) (ps)	190
Elliptical shape laser beam dimension (mm)	1.5 x 3.5

3.1.2 High Rate Imager (HRI) delay unit

When the excitation pulse occurs, the HRI module receives a trigger signal from the laser controller. This HRI delay unit is vital for acquiring a fluorescent signal in different areas of the fluorescence decay curve. This unit is essential because it is responsible for generating a delayed trigger signal sent to the HRI before starting the acquisition. The HRI trigger delay unit signals have a repetition rate from 20 MHz to 80 MHz. It also has a resolution of 1ps and a delay range of 0 to 50ns. This unit is from Kentech Instruments (Kentech Instruments Ltd., Wallingford, England), as shown in Figure 3.3.

The delay unit receives its input from the laser controller and sends its output to the HRI control module. Its control is done on the computer using dedicated software. The delays are set via RS232 interface [36].

Figure 3.3: HRI delay module.

3.1.3 High Rate Imager (HRI)

The HRI system is separated into two units, the PicoStar HR gated image intensifier and its HRI control module, Figure 3.4a and 3.4b, respectively. PicoStar HR is from LaVision (LaVision GmbH, Gröningen, Germany) and HRI module is from Kentech Instruments (Kentech Instruments Ltd., Wallingford, England).

(a) PicoStar HR. **(b)** HRI controller.

Figure 3.4: High rate imager modules used on the setup.

The PicoStar HR is an image intensifier GOI (Gated Optical Intensifier). This GOI consists of an S25 photocathode, a Microchannel Plate Detector (MCP), and a P43 phosphor screen [36].

The HRI control module is responsible for creating the temporal gates to the acquisition and controlling the MCP gain. The HRI gain is controlled by the MCP's voltage (Umcp), that defines the electrical field within the intensifier.

Figure 3.5 shows the spectral quantum efficiency(%) and the spectral cathode's photoresponse(mA/W). The luminous sensitivity is 343 μA/Lumen [36].

The parameters of the HRI module, crucial to time-gated fluorescence microscopy, are controlled by the user computer, via RS232 interface.

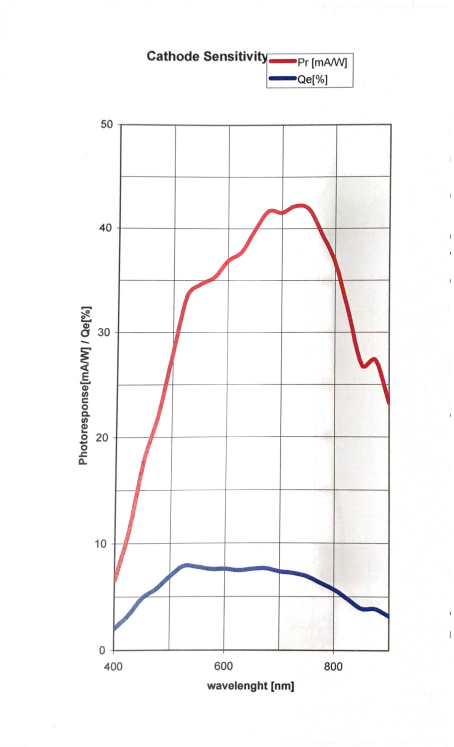

Figure 3.5: Quantum efficiency(%) and the cathode's photoresponse(mA/W) in order to the wavelength [36].

3.1.4 CCD camera

The acquisition and digitalization of the image signal is done by the Imager Compact CCD camera, from LaVision LaVision (see Figure 3.6).

The electrical signal is digitalized with a 12-bit intensity resolution. The data is then transferred to the computer's PCI (Peripheral Component Interconnect) board. The PC RAM defines the maximum number of images that can be held. It is necessary to mention that the performance of the CCD regarding the actual sample data depends on the HRI [36].

Figure 3.7 shows the spectral response of the VGA CCD sensor, and table 3.2 its technical specifications [36].

Figure 3.8 and table 3.3 shows overall gain of the microscope detector, expressed in ADC output counts in order to the electrons produced at the photocathode [36]. This includes contributions of the MCP, the CCD camera, and the camera ADC.

Figure 3.6: Imager compact CCD camera.

Table 3.2: Imager compact CCD specifications [36]

CCD	
Number of pixel	640 (H) x 480 (V)
Pixel Size (μm x μm)	9.9 x 9.9
Scan area (μm x μm)	6.3 x 4.8
Scan Rate (MHz)	12.5
Readout noise (e^-)	13-14
A/D-converter (bits)	12
Spectral range bandwith (nm)	280 - 1000
Spectral range color	primary color, RGB

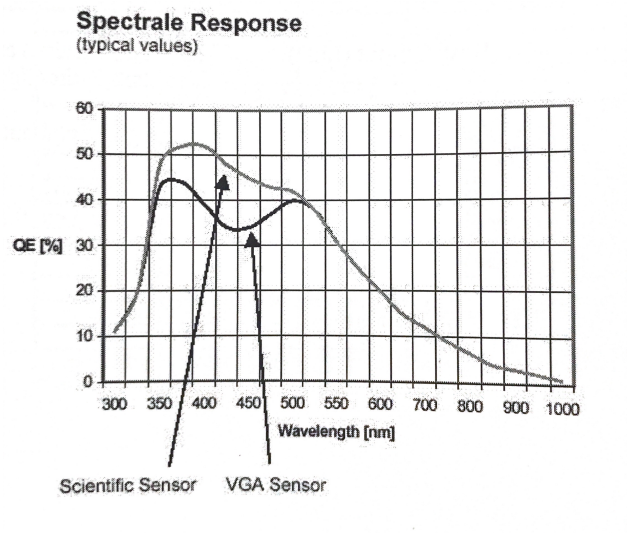

Figure 3.7: Spectral response of the VGA sensor [36].

Table 3.3: HRI gain (counts / e^-) for different voltages applied to the MCP [36].

Umcp (V)	Gain [cnts / e^-]
260	0.01
300	0.02
350	0.06
400	0.17
450	0.43
500	1.05
550	2.41
600	5.2
650	11.1
700	21.6
750	45
800	83
850	140

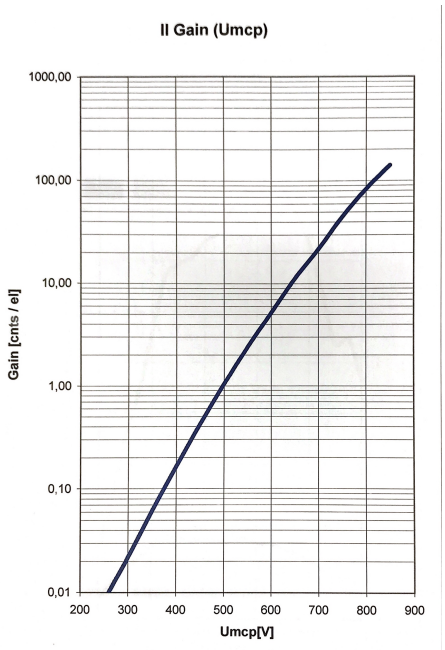

Figure 3.8: MCP gain (counts / e^-) as a function of the voltage applied to the MCP (Umcp) [36].

3.1.5 DaVis software

DaVis software enables the users to control the HRI delay unit, the HRI controller module, and the CCD. After setting all the information, the user can see the acquisition in real time.

Crucial parameters to acquire good data are the CCD acquisition time, the voltage gain of the HRI, and the gate width of the HRI [37].

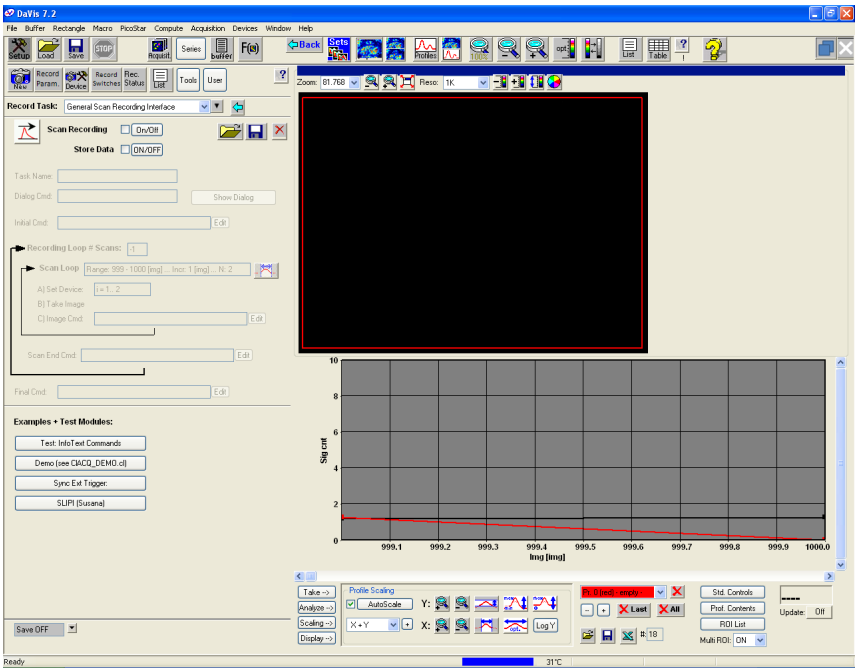

Figure 3.9: DaVis software interface.

3.2 Optical setup

The optical setup can be separated into two main parts: excitation and detection. Figure 3.10 shows schematic of the optical setup.

The excitation part is responsible for implementing the light-sheet illumination technique. The blue laser light goes first through two spherical lenses (1 and 2) responsible for expanding the beam. Next, the light sheet is created by a cylindrical lens (3) and coupled to the sample through a microscopy objective (4).

The detection part contains another microscope objective (A), for collecting the photons emitted and scattered by the sample, spectral filters (B), for rejecting excitation photons scattered by the sample, and a tube lens (C) for relaying the fluorescence photons to the gated-intensified CCD camera.

3.2.1 Optical components

The optical setup contains four discrete lenses and two microscope objectives. The following subsections are based on Figure 3.10.

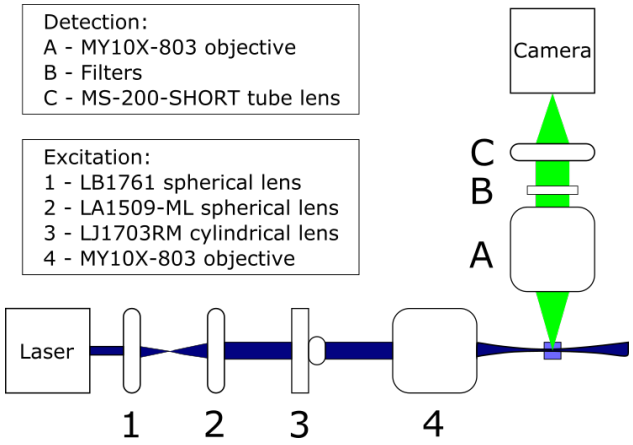

Figure 3.10: Schematic of the optical setup.

3.2.1.1 Spherical and cylindrical lenses

The initial shape of the laser beam is not adequate to create a light-sheet. Therefore, it is necessary to shape it before the beam reaches the back focal plane of the excitation objective. Firstly, a beam expander is implemented by two spherical lenses (1 and 2), LB1761 and LA1509-ML.

The cylindrical lens (3), LJ1703RM, was used to help create the light sheet. These lenses have optical power in only one direction and do not affect the light in the perpendicular dimension. Since the laser beam is already horizontally elliptical, we just need to use one cylindrical lens. Thus, this lens generates a vertical light line that fills the excitation objective back aperture, controlling the height of the light sheet [38].

Figures 3.11 and 3.12 shows the three lenses and the respective specifications are listed in table 3.4. All lenses are from Thorlabs (Thorlabs GmbH, Munich, Germany).

(a) LB1761 lens **(b)** LA1509-ML lens **(c)** LJ1703RM lens

Figure 3.11: Lenses used in the microscope excitation path.

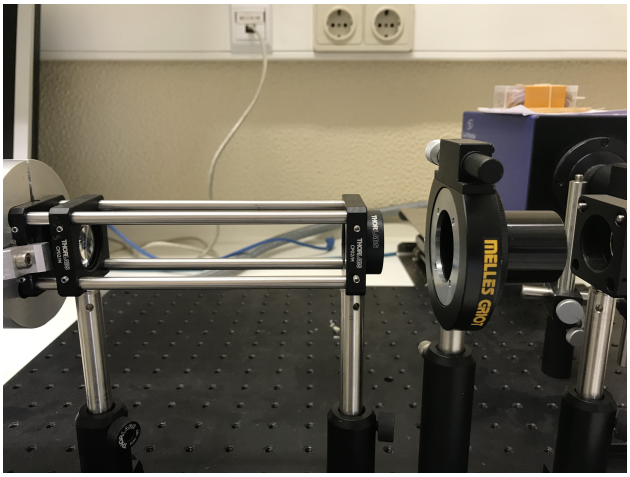

Figure 3.12: Detail of the optics on the exciation path. The beam expander is on the left. The cylindrical lens is mounted on a micrometric precision holder for accurate placement of the its power axis.

Table 3.4: Specifications of the spherical and cylindrical lenses.

	LB1761	LA1509-ML	LJ1703RM
Classification	Bi-convex spherical	Plano-convex spherical	Plano-convex cylindrical
Design wavelength (nm)	587.6	587.6	587.6
Focal length (mm)	25.3	99.7	75.0
Working distance (mm)	x	93.5	66.4

3.2.1.2 Microscope objectives

We used the same type of objective in the illumination (4) and detection (A) setup, the infinity-corrected MY10X-803. This objective from Thorlabs (Thorlabs GmbH, Munich, Germany) is shown in Figure 3.13. These objectives were one modification done on the current version of the instrument. The MY10X-803 objective is specified in table 3.5

For the illumination optics, the goal is to create the light sheet illumination that will excite the sample. Compared to the LSM04-BB telecentric objective used in the previous version of the instrument, the current objective represents a significant improvement by providing a larger numerical aperture (NA). In addition, given the light source characteristics, the optimal wavelength range is now matched to the objective, resulting in much better transmission efficiency. All the specifications are presented in the table 3.5.

In the case of the detection setup, the previous system had severe restrictions concerning sample placement, due to the very short working distance (WD) of the

two objectives then used (1,2mm and 0,6mm). The current detection objectives correspond to a very significant improvement of the instrument usability, by providing a substantially larger working distance.

Figure 3.13: Microscope objectives MY10X-803.

Table 3.5: Objective specifications.

MY10X-803	
Magnification	10x
Numerical Aperture	0.28
Optimal wavelength range (nm)	436 - 656
Working Distance (mm)	34
Effective focal length (mm)	200

3.2.1.3 Optical filters

Optical detection filters (B) are vital in fluorescence imaging instruments. This component assures that the only photons reaching the detector are fluorescence photons. Therefore, they must block the scattered excitation photons.

As said before, the sample's emission wavelength range is between 520 and 570 nm. Therefore, the ideal filter should have a transmission as high as possible in this range, and as low as possible for the excitation wavelengths. In this case, in Figure 3.14, the detection filter's spectral response blocks most unwanted wavelengths [1].

3.2.1.4 Tube lens

The tube lens function is to focus the collimated beam, exiting the infinity-corrected detection objective, forming an image of the sample on the photocathode of the HRI. The MS-200-SHORT tube lens (C) with a 200 mm focal length, was used. This tube lens is from Seiwa (Seiwa Optical Europe GmbH, Frankfurt, Germany).

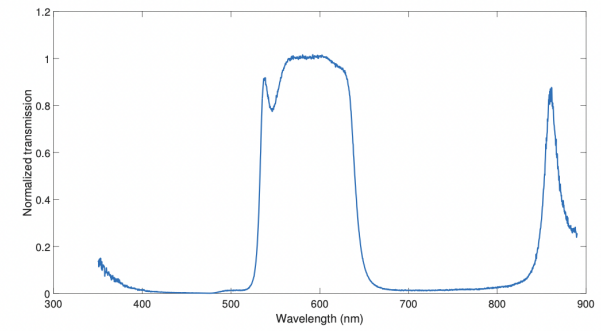

Figure 3.14: Spectral light transmission of the detection filters [1]

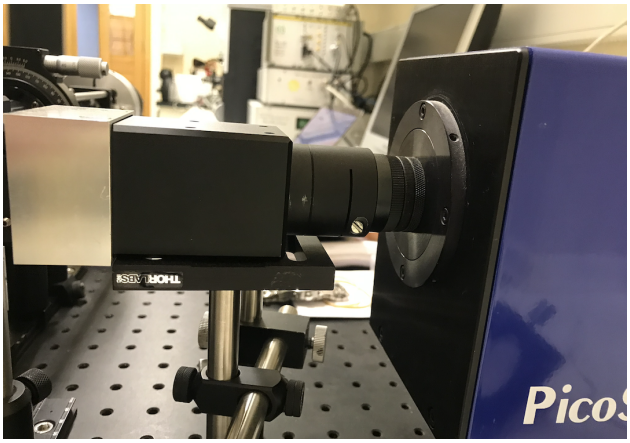

Figure 3.15: Tube lens setup.

The complete optical microscope setup is shown in Figure 3.16.

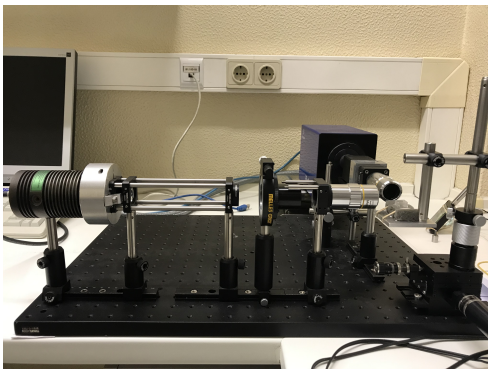

(a) Side view.

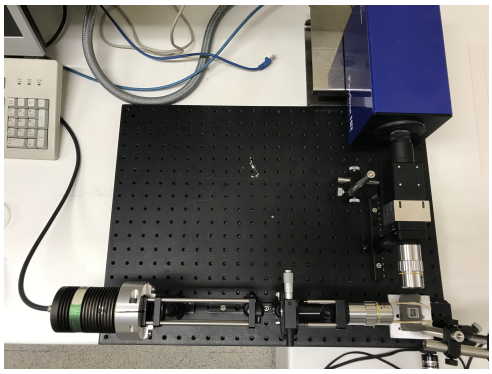

(b) Top view.

Figure 3.16: Setup images from two different perspectives.

3.3 Sample positioning and sectioning

Positioning control of the sample is done by two actuators that allow the user to move the sample on the x (detection) and y-axis (illumination) with reasonable accuracy:

on the x-axis, the T-LA28A from Zaber (Zaber Technologies Inc., Vancouver, Canada) and, on the y-axis, the MT1A from Thorlabs (Thorlabs GmbH, Munich, Germany).

The T-LA28A has a micro-step of 0.0992 μm and a range of 28 mm. The software from Zaber was used to control this device through an RS-232 communication interface. The movement of the sample on the x-axis, through the excitation light sheet, provides optical sectioning of the sample. On the other hand, the MT1A is a manual actuator. It consists of a translational stage platform with a 0.5 μm displacement per single rotation and a 12.7 mm travel range. These two elements are crucial to placing a sample area on the focal plan.

4

Microscope evaluation

Before starting the imaging trials, it is essential to assess the performance of the designed system. Therefore, this chapter is divided into subsections evaluating optical and timing parameters. Field of view, lateral and axial resolution were the optical parameters assessed to determine if the microscope fulfilled the initial requirements. Fluorescent solutions with well-known fluorescence lifetimes were studied to evaluate the timing accuracy of the system.

4.1 Field of view

Field of view (FOV) can be defined as the physical area that the microscope can image. This parameter depends on the properties of the detection objective, and CCD Camera [39]. FOV was measured for the MY10X-803 infinity-corrected microscope detection objective.

The method used to measure this parameter was using the 1951 USAF resolution test target from Thorlabs (Thorlabs GmbH, Munich, Germany). This test target comprises multiple groups of dimension-known element bars. Each group has six elements, and each element is composed of three same-sized horizontal and vertical bars—the higher the group number, the smaller the bars. This also applies to the groups. The widths of the bars range goes from 2.00 x 10^{-3} μm to 4.38 x 10^{-6} μm [40].

The target was illuminated by a green light -the same wavelength as the fluorescence photons under study- and placed at the objective focal plane. Acquired images are then processed and used to measure the FOV of the microscope.

4.1.1 Angle determination

Before FOV measurement, it was essential to verify the alignment between the target and the detection unit. We measured the FOV by determining the size of each image pixel, using the known dimensions of the 1951 USAF target elements. So, if the target is rotated by an angle α in relation to the detection unit, the measured value of FOV is not an accurate estimation of the real FOV. Figure 4.1 illustrates this condition for a single element of the test target.

The procedure to calculate α was simple. Using MATLAB® (The MathWorks Inc., Natick, Massachusetts, United States), we selected two points that were supposed to be aligned—for example, selecting the top left and top right corner of a given bar. This way, knowing the (X, Y) coordinates of each point, we could determine if there is a rotation on the target. The value of α was calculated using the simple equation $\tan \alpha = \frac{y_2 - y_1}{x_2 - x_1}$. The method of selecting the points is not completely precise, but it is a reasonable approximation. This procedure was repeated seven times for each axis. Table 4.1 presents the mean and standard deviation of α relative to x-axis.

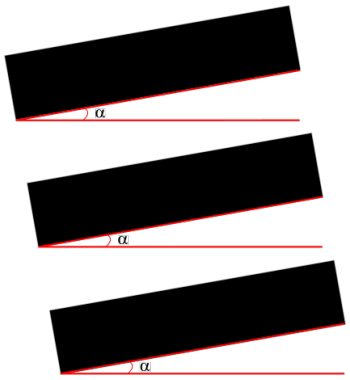

Figure 4.1: Rotation by an angle alpha between the test target and the detecion unit.

Table 4.1: Angle of rotation for both objectives.

Target angle of rotation	
Angle of rotation (degrees)	1.547 ± 0,003

4.1.2 FOV determination

Determining FOV is a basic association procedure. The tricky part is calculating the number of pixels corresponding to a single bar. As we know the value of any selected bar's dimensions, given by the test target specifications, we need to know

how many pixels correspond to those dimensions. As we already know, the CCD has 640 pixels on the x-axis and 480 on the y-axis. Given this, it is then easy to calculate the FOV. The value of FOV is easier to calculate and more reliable for larger bars. Figure 4.2 shows the image of the target test obtained by the microscope.

As mentioned, the tricky part is to select the valid pixels for a given bar. This selection was made by setting a threshold based on the greyscale. The threshold value must be accurate because it will define the limits of what is and isn't representative of the bar. The pixel dimension was calculated six times for each axis, and the measured FOV values are presented in table 4.2.

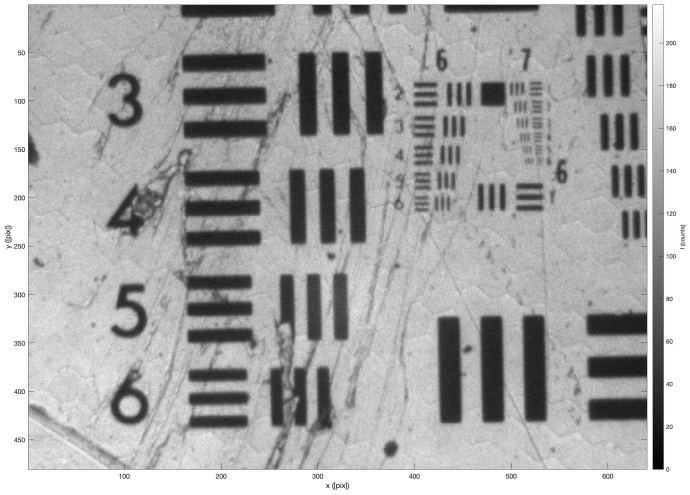

Figure 4.2: Target test image with MY10X-803 objective.

Table 4.2: Microscope Field of View. Values are mean ± standard deviation.

MY10X-803 objective FOV	
x-axis (μm)	876 ± 40
y-axis (μm)	652 ± 20

4.2 Lateral resolution

The lateral resolution may be defined as the separation distance at which two objects are imaged with a specific contrast value. Theoretically, this resolution can be determined by the equation:

$$R.lateral = \frac{0.61\lambda}{NA} \tag{4.1}$$

where λ is the wavelength and NA is the Numerical aperture of the detection objective [41, 23, 42].

The lateral resolution of the microscope was also measured using the USAF 1951 test target. The image of this target, shown in Figure 4.2, was acquired for a gain of 260 V.

According to the Rayleigh criterion, when the condition of minimum separation occurs, the contrast between the point spread functions (PSF) and the valley between the two neighboring peaks is 26.4%. This condition of relative amplitude of peaks and valleys intensities determines the lateral resolution [43, 41, 23].

MATLAB® *improfile* function was used to analyze images obtained with the test target. This function allows the user to draw a perpendicular line over the bars of the test target and then plot the intensity profile along that line. For the x-axis, the element and group number closer to the 26.4% contrast limit was group 7 and element 2. For the y-axis, it was group 7 and element 1. The corresponding lateral resolution values are shown in table 4.3. Images A.1 and A.2 show the plots of the intensity for both axis. The precision of this measurements is hampered by the reduced number of data points used to obtain the intensity profiles.

Table 4.3: Lateral resolution values.

MY10X-803 objective	
x-axis resolution (μm)	< 3.48
y-axis resolution (μm)	< 3.91

4.3 Axial resolution

The axial resolution is a crucial parameter in this study. This parameter is related to the optical sectioning capacity of the microscope. Optical sectioning is the capacity of imaging thin slices of the sample, getting a signal just from a thin plane coinciding with the focal plane of the detection unit [23]. As this project aims to image transparent tissues with a thickness of around 500 μm, it is essential to be capable of imaging much smaller slices.

Green fluorescent microspheres (Thermo Fisher Scientific, Massachusetts, EUA) were used to measure the axial resolution. These polystyrene microspheres have a 2.9 μm diameter and the same emission and absorption spectra matching the illumination and detection bands of the microscope as the system. Observing

stable microspheres was only possible by embedding them on agarose phantoms. Moreover, these phantom enables the retention of the microspheres in a transparent and nonfluorescent environment. Given these advantages, two phantoms of different quantities of microspheres were prepared.

The method consists of imaging a series of images of the microspheres while scanning the sample along the axial direction, through the focal and illumination plane of detection. The data is then analyzed, fitting the axial intensity distribution for one particular to an adequate peak function and calculating the Full Width at Half Maximum (FWHM) of that function. The FWHM can be regarded as the axial resolution. This procedure is commonly used and effective in measuring axial resolution in fluorescence microscopy [23, 44, 45]. The small-step axial scan is implemented with the T-LA28A actuator.

After the acquisitions, MATLAB® ROI (region of interest) tools were used to obtain the intensity of a selected microsphere. First, a microsphere was chosen. After that, an 8x8 pixel ROI was used to obtain the intensity sum of all the pixels. Finally, the fitting was done on OriginLab software.

Gaussian and Lorentzian functions were used to fit the axial intensity profile. The goodness of the fit was assessed by the reduced chi-square. The best fit was obtained with a Lorentzian function and produced an axial resolution value of 8.60 μm. The actual value of the microscope axial resolution value may be even lower, since it seems possible to image microspheres with higher stability. The measured value represents a very significant improvement over the one obtained with the previous configuration of the microscope, and it is adequate for fulfilling the goals of the project.

Figure 4.3 shows the highest intensity plane of the image volume acquired for measuring the axial resolution, while Figure 4.4 shows the lowest intensity one. A red circle identifies the selected microsphere. Figure 4.5 shows the Lorentzian fit and its parameters.

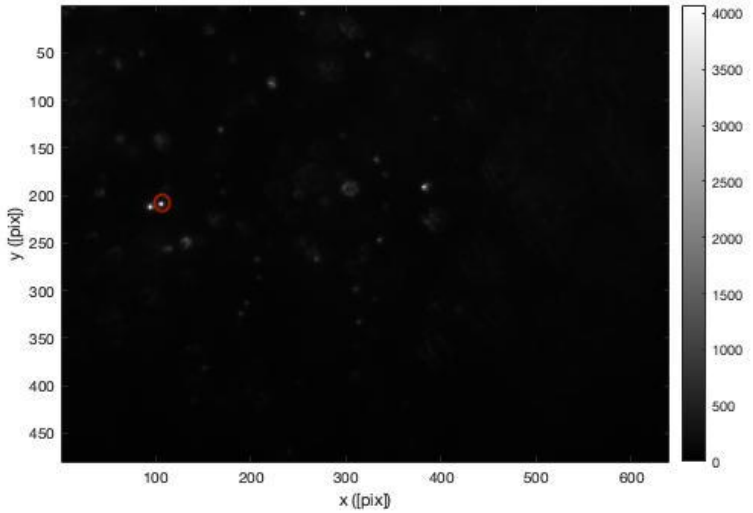

Figure 4.3: Image of the axial plane where the selected microsphere is is imaged with the highest intensity.

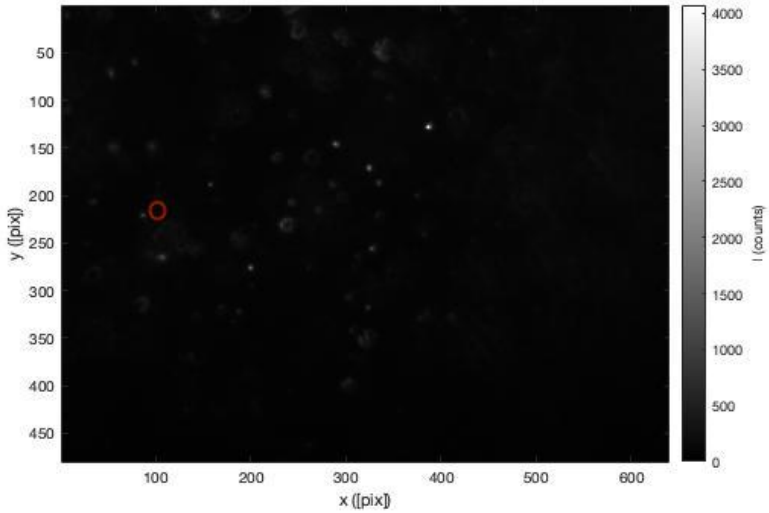

Figure 4.4: Image of an axial plane where the studied microsphere is no longer imaged.

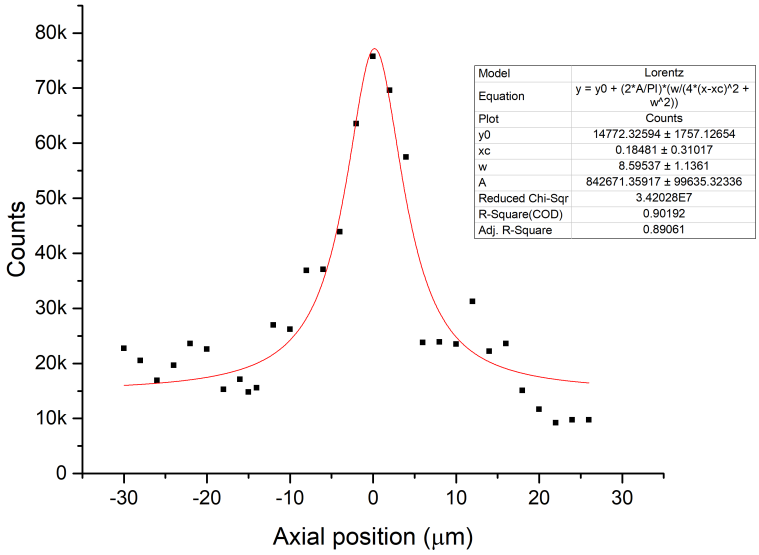

Figure 4.5: Lorentzian fit to the microsphere data and the corresponding fit parameters.

4.4 Time-resolved measurements

The software used to fit the acquired data and obtain the values of the fluorescence decay parameters is FLIMfit [1]. This free software is commonly used in FLIM studies. In FLIM, the acquired data does not correspond to the decay but to the convolution of the real decay and the instrument response function (IRF). Hence, it is obligatory to measure the IRF of the system [46, 1].

4.4.1 Instrument response function

For measuring the IRF, we used a standard fluorophore with a lifetime significantly shorter than the system time resolution. This way, the obtained signal can be considered the IRF of the system [46, 1]. The fluorophore must have absorption and emission spectra within the spectral range of our system.

A solution of Erythrosin B in water was chosen. It has a single-exponential decay with a lifetime of 90 ps. Furthermore, this solution was already successfully used for the same purpose in other studies [46].

Figure 4.6 shows the acquired data for the gate width of 1000 ps. This figure also

shows the gaussian fit to the data, yielding a temporal resolution, given by the FWHM value, of 689.96 ps [46]. IRF was also measured for other gates widths such as 900, 800, and 200 ps. Figure A.3 shows the acquisition plot for all four gates.

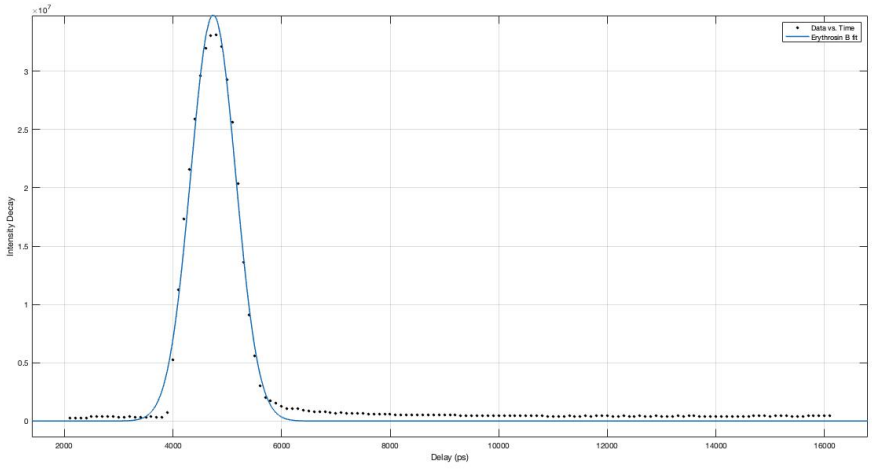

Figure 4.6: Data acquired for a solution of Erythrosin B in water and its gaussian fit. This fitting curve corresponds to IRF.

4.4.2 Timing accuracy

The timing accuracy of the Time-gated microscope was measured using well-known fluorescent samples. Coumarin 153 in methanol and Riboflavin were the chosen samples. Both solutions follow the wavelength requirements. The selected gate width was 1000 ps to acquire the maximum possible number of photons.

Figure 4.7a and 4.7b show the best fits obtained with FLIMfit for Coumarin 153 in methanol and Riboflavin, respectively. Coumarin 153 data was fitted with a mono-exponential decay function, and Riboflavin data with a bi-exponential decay function.

The goodness of the fit was evaluated by the reduced chi-square χ^2. When the theoretical module explains well the experimental data, the reduced chi-square should be approximate to one. Values significantly higher than one indicate a poor quality fit. On the other hand, values lower than one do not correspond an improvement in the fitting process. Usually they indicate insufficient statistics. In a real experiment, the reduced chi-squared is usually greater than one and is not possible to establish a threshold value defining a good fit. In TCSPC experiments, chi-square values between 0.8 and 1.2 are considered as indicators of an adequate fit. For Time-gated FLIM measurements, data fits are considered as adequate with

chi-square values higher than those accepted for TCSPC.

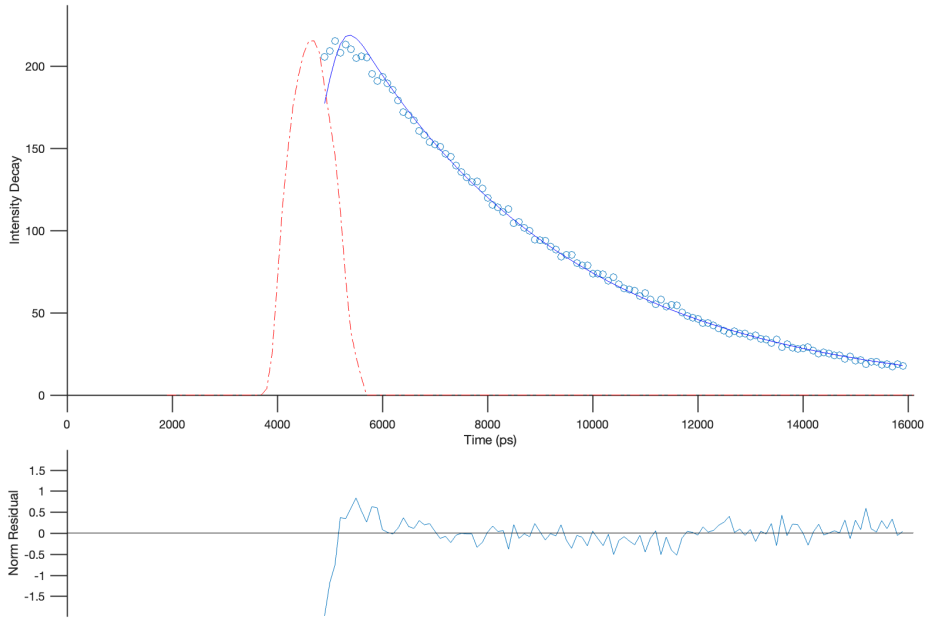

(a)

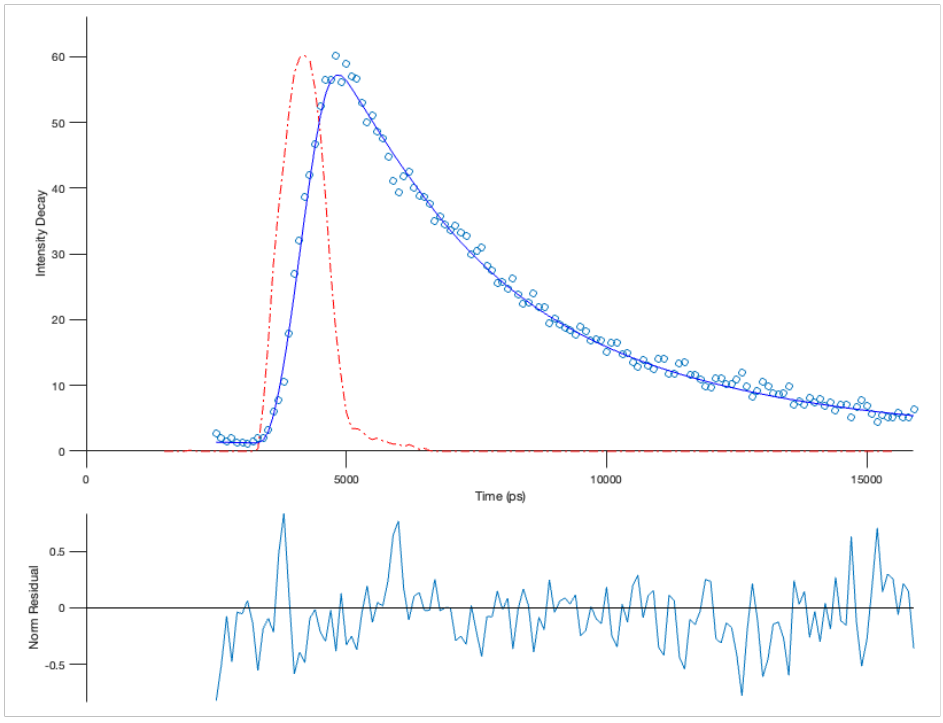

(b)

Figure 4.7: Fluorescence decay data and their fits for the test solutions used to assess the timing accuracy of the microscope: (a) Coumarim 153 in methanol; (b) Riboflavin in methanol. Fits were done using FLIMFit and included IRF deconvolution. Normalized residuals are shown for each fit.

The results obtained with the Coumarim 153 solution show a good performance of the system on measuring fluorescence lifetimes close to four times longer than the 1000 ps gate width. In addition, given the literature reference value, the fit result shows an improvement in the system timing accuracy, when compared to the previous version of the microscope [1].

The fluorescence emission of Riboflavin was fitted to a bi-exponential decay function with lifetimes τ_1 equal to 0.13 ns, τ_2 equal to 2.94 ns, with the respective pre-exponential factors β_1 and β_2 being 0.12 and 0.88. We believe that the longer lifetime component corresponds to the fluorescence emission from Riboflavin, while the fast component is probably due to contaminants since the solution was in contact with animal corneas in previous studies [46]. Another common aspect of the Riboflavin compound is the relationship between pH and the value of the fluorescence lifetime [47]. At the time of the measurement, the pH was 6.28. Table 4.4 condenses all the information about the results on both samples fit.

Table 4.4: Fluorescence lifetimes for the solutions used to assess timing accuracy. The goodness of the fit was evaluated by the reduced chi-square χ^2. The reference values are based on literature [48, 49]. Experimental values correspond to mean ± standard deviation.

Parameters	Coumarin 153 in methanol	Riboflavin
Reference values (ns)	4.3	3.37
τ_1	4.16 ± 0.02	0.13 ± 0.04
β_1	1.0	0.12
τ_2	-	2.939 ± 0.002
β_2	-	0.88
χ^2	1.23	1.07

The aging of Erythrosin B, Coumarin 153, and Riboflavin solutions might modify their fluorescence properties and is a factor that we must consider.

Is important to note that the standard deviations of table 4.4 do not correspond to the true uncertainty on the fluorescence lifetime measurements. They only indicate the variability in the measurements obtained from a uniform sample. The true uncertainty will depend on the fluorescence lifetime resolution of the microscope. This can be inferred from the FWHM of the IRF of the microscope (689.96 ps). Deconvolution of the experimental data with the IRF allows to resolve lifetimes corresponding to a fraction of the IRF FWHM. In TCSPC it is considered a lifetime resolution of FWHM/10, for single exponential decays, and FHWM/5 for bi-exponential

decays. In Time-gated systems, the lifetime resolution is closer to the FHWM value.

5

Imaging trial results

5.1 Introduction

The main objective of the implemented microscope is the study of thick biological tissues, such as corneas. Since ex-vivo human corneas were unavailable during this study, we used porcine corneas. These corneas have similar anatomy to human ones [2].

The cornea is the most external layer of the eye. The human cornea consists of five layers: the epithelium, Bowman's layer, stroma, Descemet's membrane, and endothelium. In the case of the porcine cornea, the Bowman's layer does not exist. This means that there is no membrane between epithelium and stroma [1, 2, 50]. Figure 5.1 shows all the mentioned layers.

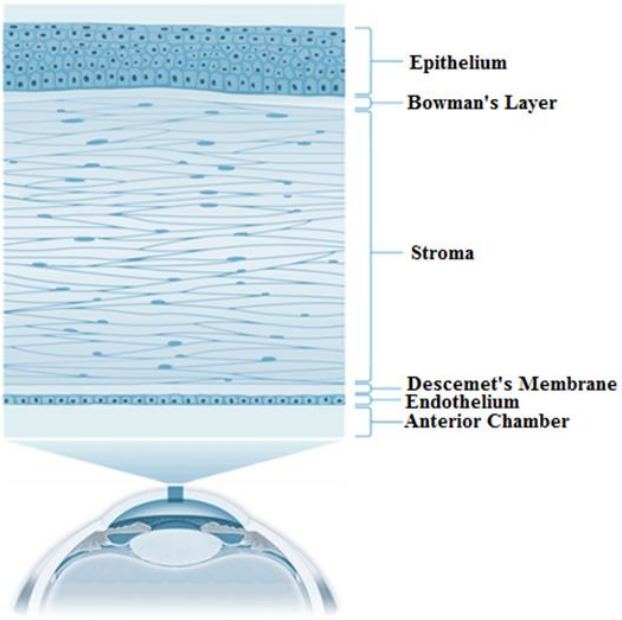

Figure 5.1: Human cornea layers representation [51].

The epithelium is composed of superficial, wing, and basal cells. The stroma

constitutes around $\sim$ 90 % of the porcine cornea and more than 85% of the human one. Its composition is mainly collagen fibrils. The Bowman's layer and Descemet's membrane are composed of collagen and glycoproteins. Descemet's membrane usually is thinner than Bowman's layer. Lastly, the endothelium is a single layer of cells. These cells usually have a standard form and dimensions [1, 50].

Table 5.1: Differences between the layers thickness of human and ex-vivo porcine cornea [1, 2].

Cornea layer	Human (μm)	Porcine (μm)
Epitelyum	$\sim$ 50 - 52	$\sim$ 80
Bowman's layer	8 - 10	-
Stroma	$\sim$ 470	$\sim$ 900
Descemet's membrane	$\sim$ 7	$\sim$ 30
Endothelium	4 - 6	
Total	$\sim$ 540	$\sim$ 1010

Since we had to wait a long time before imaging animal corneas, we tried other solutions to image biological tissues. The most reasonable solution was onion imaging due to its characteristics.

5.2 Onion imaging

Onions have a relatively transparent layered structure. We also decided to test the microscope in reflectance mode, that is, without optical filters mentioned in 3.2.1.3, since onions do not exhibit intense fluorescence.

5.2.1 Non-fluorescence imaging

The acquisitions in reflectance mode were quite good. We were able to image onion cells. Figures 5.2, 5.3, 5.4, and 5.5 show the acquisitions for the axial depth of 0, 54, 105, and 147 μm, respectively. We assume Figure 5.2 as the reference image plane.

As we see, the onion cell layer is the same for all the acquired figures. This is because the onion was imaged on a cornea holder. Figure 5.6 shows how the onion was fastened to the holder. This holder helps the sample maintain a curved shape. As the onion is curved, it was necessary to move the cells through the focal plane using small axial steps.

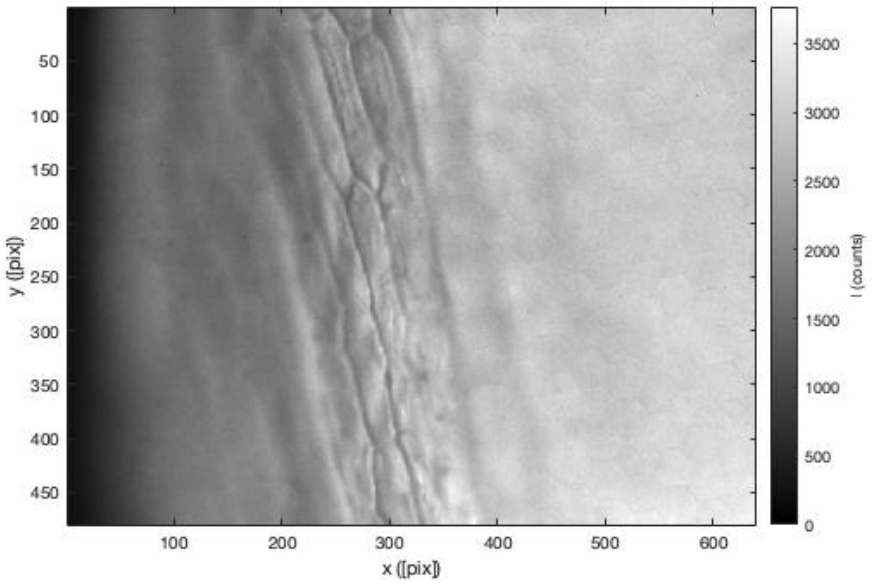

Figure 5.2: Onion cells. This image was used as a reference plane (z=0 μm).

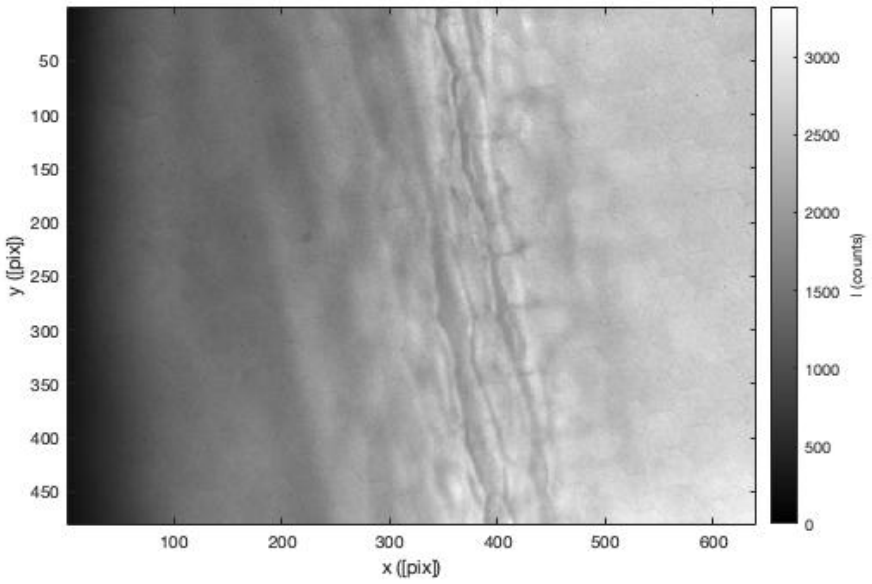

Figure 5.3: Onion cells. This image was at a distance of 54 μm from the reference plane.

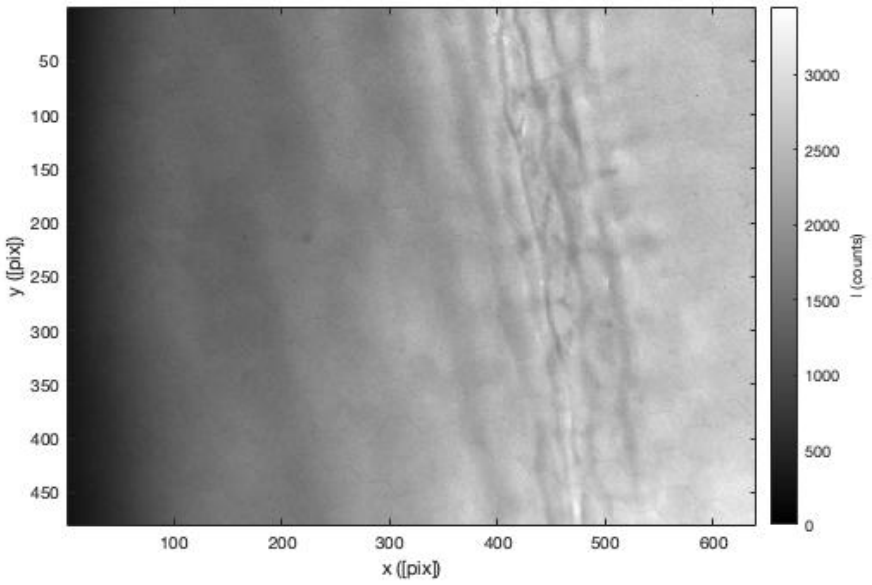

Figure 5.4: Onion cells. This image was at a distance of 105 μm from the reference plane.

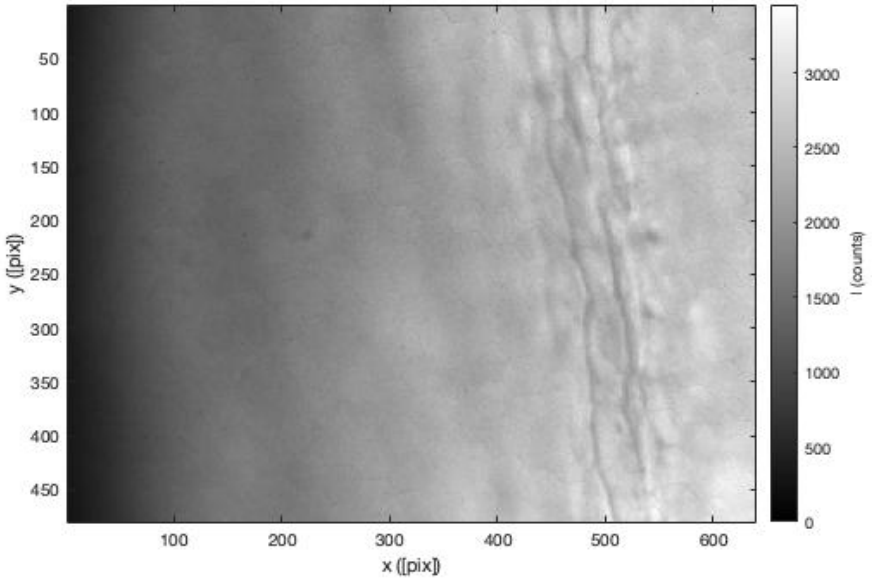

Figure 5.5: Onion cells. This image was at a distance of 147 μm from the reference plane.

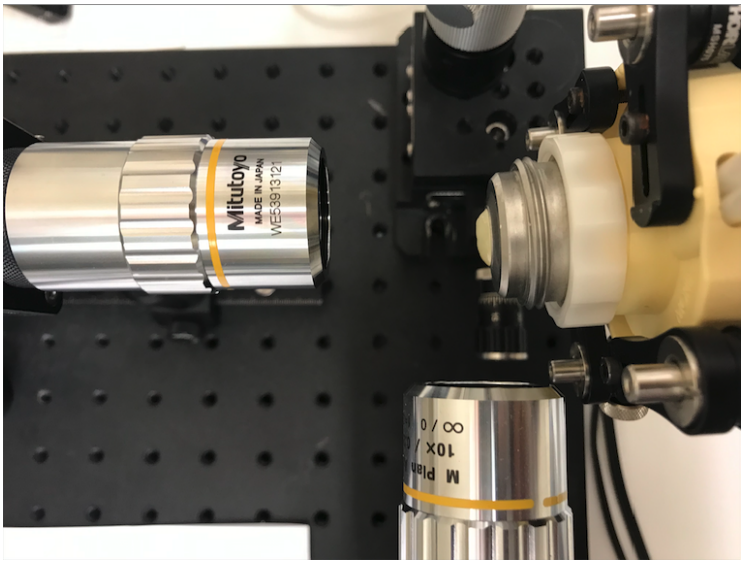

Figure 5.6: Cornea holder setup used to image the onion.

5.2.2 Fluorescence imaging

As mentioned, onions do not have significant natural fluorescence properties. Due to that, we placed the sample onion partially in contact with a solution of Coumarin 153 in methanol. We studied this solution in section 4.4.2.

Figure 5.7 shows that we can image the superficial onion cells with a fluorescence signal. The cell structure can be imaged with reasonably good contrast.

For the same acquisition, we measured the value of the fluorescence lifetime. We expected that the fluorescence lifetime was roughly identical to the one presented in section 4.4.2. The best fit to the acquired data was obtained with a bi-exponential decay function. The decay parameters are shown in table 5.2. These results show that the chi-squared value is high. The value of τ_1 is similar to the one previously measured for Coumarin 153. The second decay component, which exhibits a shorter lifetime, might result from an interaction between the onion molecules and the Coumarin solution. Measurements done on natural onion cells (i.e. not instilled with Coumarin) revealed a very weak signal which most probably will influence this results.

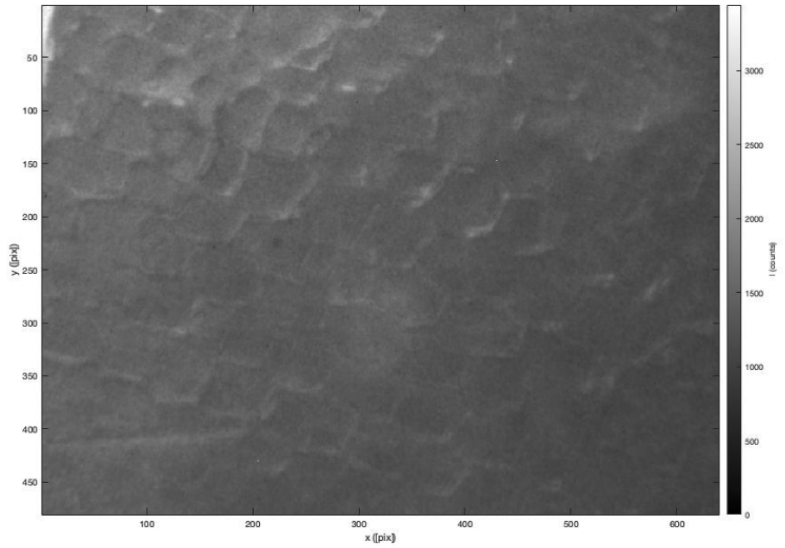

Figure 5.7: Onion fluorescence imaging. The fluorescence properties are due to the partial immersion of the onion in a Coumarin 153 solution.

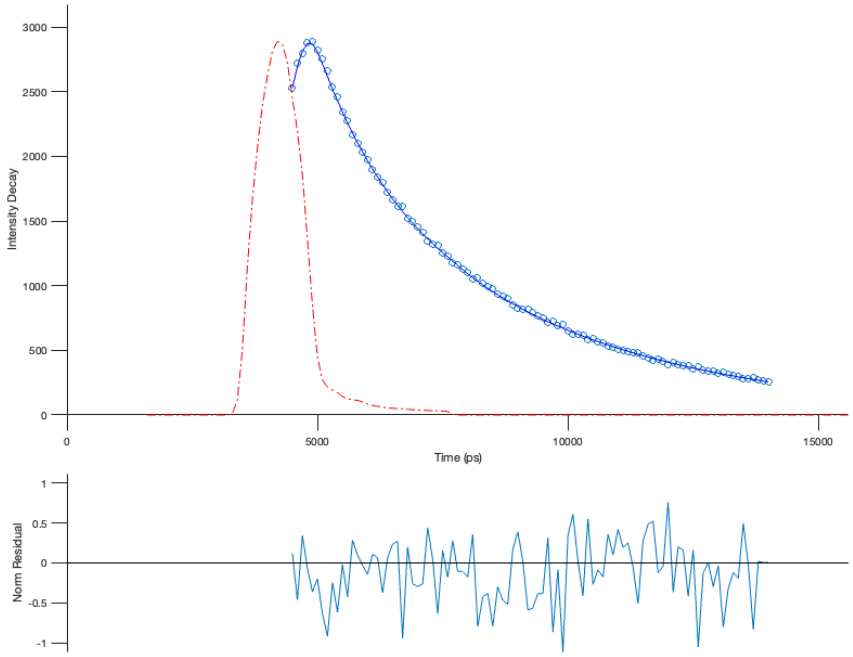

Figure 5.8: Fluorescence decay data and respective fit for the onion sample.

5.3 Porcine cornea imaging

The ex-vivo porcine cornea imaging was done only for the epithelium. The goal was to obtain the fluorescence signal of FAD, described by a bi-exponential decay function. Several values of MCP gain and exposure time were evaluated. The best combination was to set MCP gain to 550V and an exposure time of 5.0s. The

Table 5.2: Fluorescence lifetimes for onion cells in contact with Couramin 153 in methanol. The goodness of the fit was evaluated by the reduced chi-square χ^2. The reference values are based on the results previously obtained in section 4.4.2. Values correspond to mean ± standard deviation.

	τ_1 (ns)	β_1	τ_2 (ns)	β_2	χ^2
Onion with Coumarin 153	4.33 ± 0.06	0.49 ± 0.01	0.97 ± 0.05	0.51 ± 0.01	5.00

cornea was placed on the mentioned cornea holder, and viscoelastic gel was used to maintain the cornea's natural curved shape.

Figure 5.9 shows the highest intensity plane of the porcine epithelium volume acquired. The figure shows that we cannot see the epithelium cells. This shows that the optical sectioning and the contrast are still insufficient to obtain the desired results.

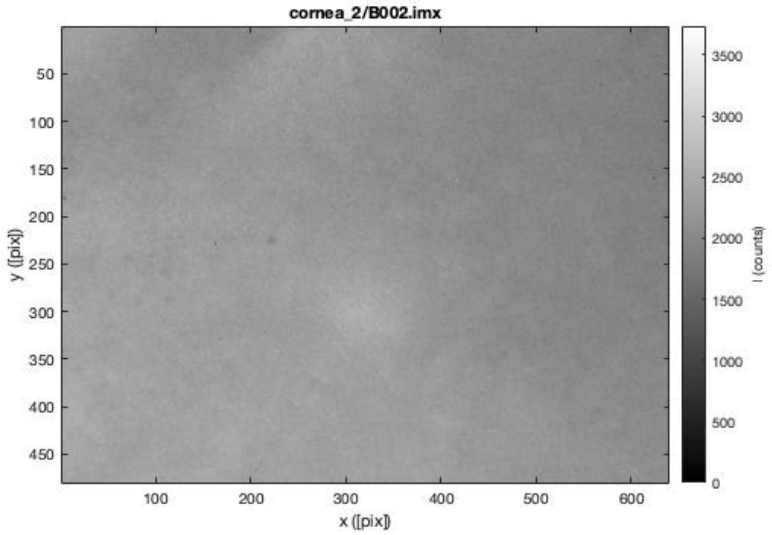

Figure 5.9: Image of the porcine epithelium plane with the highest intensity.

We also measured the fluorescence lifetime of the epithelium. The intensity data were fitted to a bi-exponential decay function. The results are summarized in table 5.3. Figure 5.10 shows the data, and the respective fit made using FLIMfit software.

There are significant differences when comparing the measured values of fluorescence lifetime of FAD in porcine corneas with the reference ones. For example, we see that for τ_1, the accuracy error is around 38%, and for τ_2 is around 25%.

Several factors may contribute to the differences between measured and reference values. Optical sectioning is larger than one cell layer. That means we can have

Table 5.3: Fluorescence lifetimes for porcine cornea. The goodness of the fit was evaluated by the reduced chi-square χ^2. The reference values are based on other studies which used porcine corneas [50]. Values correspond to mean ± standard deviation.

	τ_1 (ns)	β_1	τ_2 (ns)	β_2	χ^2
Porcine epithelium	3.78 ± 0.03	0.242 ± 0.003	0.69 ± 0.01	0.758 ± 0.003	1.25
Reference values	2.47 ± 0.89	-	0.55 ± 0.07	-	-

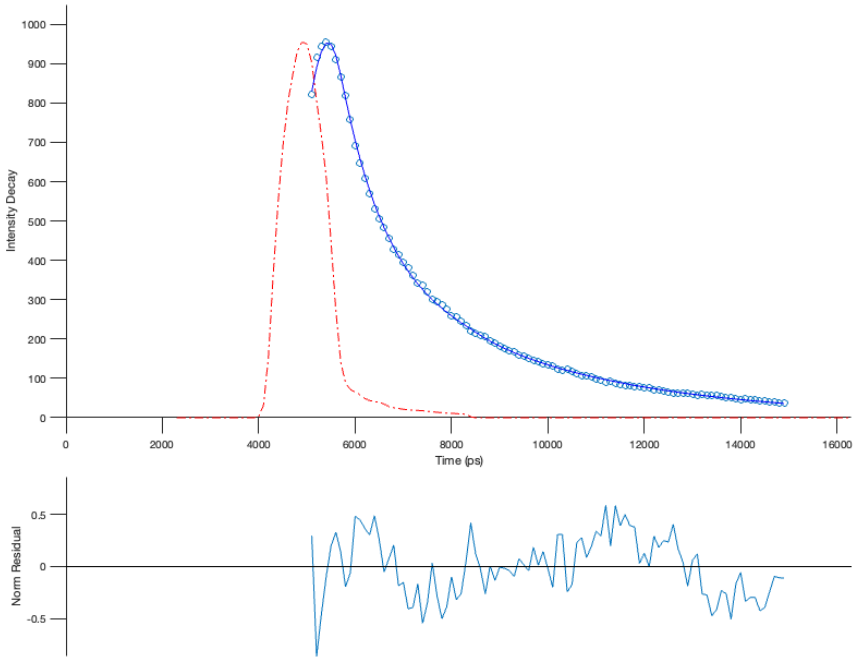

Figure 5.10: Fluorescence decay data and respective fit for the fluorescence porcine epithelium.

different layers, with different metabolic activity, emitting photons, leading to signal overlap and decreasing fluorescence lifetime accuracy. On the other hand, it is known that a living cornea has a naturally low concentration of FAD. Given that we imaged an ex-vivo cornea, the fluorescence signal is necessarily lower [13]. This leads to the necessity of imaging with a longer exposure time. This may cause irreversible losses in the fluorescence properties of the fluorophores due to photobleaching.

Even though the results were not as good as we would like, it is essential to mention that they were better than those obtained with the previous version of the microscope. This gives the confidence to keep developing the system.

6

Conclusions

6.1 Discussion and conclusions

The system aimed to measure thick biological tissues' FAD fluorescence signals. To do this, it uses a 440 nm central wavelength laser to excite the fluorophores and collects the fluorescence photons that are emitted between 520 and 570 nm.

About the microscope evaluation, it was expected that FOV results were higher when compared to the previous version of the microscope, since the detection objective changed [1]. This new objective magnification reduction led to a greater FOV than the initial requirements. This does not affect negatively the microscope performance since the samples will be larger than the estimated FOV.

The initial requirement for lateral resolution was to obtain a result smaller than 20 μm. Given that for both axes, we got less than 80% of that reference values, the requirement is fulfilled.

The axial resolution results provided at least 14 to 42% better resolution than required. Microspheres imaging tests showed that axial resolution and light-sheet thickness significantly impact optical sectioning.

The last item to review was the timing accuracy. The errors relative to the reference values for Coumarin 153 and Riboflavin samples were, respectively, 3,3 % and 12.8%. The justifications given in the previous section support the claim that the system has a reasonably good timing accuracy. In addition, the ability to measure the fluorescence signal from samples showed that the system is operational. With that said, it was considered that this system was ready for imaging trials.

The imaging trial with onions was a good indicator that the development of this project should move forward. The trials with porcine cornea show that we can still not image the cells, due to the lack of adequate contrast. In addition, the fact that the ex-vivo porcine cornea has a low concentration of FAD makes imaging the

fluorescence signal even more difficult. The measured FAD fluorescence lifetime is not similar to the reference values. The lack of adequate rejection of out-of-focus signal leads to insufficient performance of the detection system in tissues like porcine corneas.

We consider that, compared with the previous study [1], the changes in the system improved essential parameters like the working distance, axial resolution, and optical sectioning. However, even though there were improvements, the system is still unable to perform as required.

6.2 Future work

This study is the second implementation of light-sheet illumination in this group. Combining this kind of illumination with Time-gated acquisition is a challenging project requiring considerable development time to achieve the required performance.

We must improve sample positioning methods. Since we have only one sample axis controlled via software, it would be a significant improvement if that could also be done for the other two axes. A rotational sampling plate would also be interesting because it would help get better optical sectioning. When we acquired, for example, the microspheres signal, it was challenging to stabilize the phantom. Getting better and more stable holders that are not available in the laboratory is essential.

Finally, as mentioned throughout the dissertation, the main goal is to improve the optical sectioning and contrast. It would also be interesting to test the system with human ex-vivo corneas.

References

[1] A. Í. D. Machado, *Time-gated fluorescence lifetime microscope with light-sheet illumination*. PhD thesis, Universidade de Coimbra, 2021.

[2] I. Sanchez, R. Martin, F. Ussa, and I. Fernandez-Bueno, "The parameters of the porcine eyeball," *Graefe's Archive for Clinical and Experimental Ophthalmology*, vol. 249, no. 4, pp. 475–482, 2011.

[3] T. W. Smith, "Corneal topography," *Documenta Ophthalmologica*, vol. 43, no. 2, pp. 249–276, 1977.

[4] T. Swartz, L. Marten, and M. Wang, "Measuring the cornea: the latest developments in corneal topography," *Current opinion in ophthalmology*, vol. 18, no. 4, pp. 325–333, 2007.

[5] J. P. Whitcher, M. Srinivasan, and M. P. Upadhyay, "Corneal blindness: a global perspective," *Bulletin of the world health organization*, vol. 79, no. 3, pp. 214–221, 2001.

[6] E. B. van Munster and T. W. Gadella, "Fluorescence lifetime imaging microscopy (flim)," *Microscopy techniques*, pp. 143–175, 2005.

[7] F.-J. Meyer-Almes, "Fluorescence lifetime based bioassays," *Methods and applications in fluorescence*, vol. 5, no. 4, p. 042002, 2017.

[8] V. Mannam, X. Yuan, and S. Howard, "Deconvolution in fluorescence lifetime imaging microscopy (flim)," *arXiv preprint arXiv:2201.06136*, 2022.

[9] J. R. Lakowicz, *Principles of fluorescence spectroscopy*. Springer, 2006.

[10] W. Yang and S.-L. Chen, "Time-gated fluorescence imaging: advances in technology and biological applications," *Journal of Innovative Optical Health Sciences*, vol. 13, no. 03, p. 2030006, 2020.

[11] J. W. Lichtman and J.-A. Conchello, "Fluorescence microscopy," *Nature methods*, vol. 2, no. 12, pp. 910–919, 2005.

[12] A. Sharma and S. G. Schulman, *Introduction to fluorescence spectroscopy*, vol. 13. Wiley New York, 1999.

[13] S. F. Silva, *Time-Gated Fluorescence Lifetime Microscopy Methods and Instrumentation for Metabolic Imaging*. PhD thesis, 00500:: Universidade de Coimbra, 2019.

[14] N. Boens, W. Qin, N. Basarić, J. Hofkens, M. Ameloot, J. Pouget, J.-P. Lefevre, B. Valeur, E. Gratton, M. VandeVen, *et al.*, "Fluorescence lifetime standards for time and frequency domain fluorescence spectroscopy," *Analytical chemistry*, vol. 79, no. 5, pp. 2137–2149, 2007.

[15] P. I. Bastiaens and A. Squire, "Fluorescence lifetime imaging microscopy: spatial resolution of biochemical processes in the cell," *Trends in cell biology*, vol. 9, no. 2, pp. 48–52, 1999.

[16] W. Becker, *Advanced time-correlated single photon counting techniques*, vol. 81. Springer Science & Business Media, 2005.

[17] L. M. Hirvonen and K. Suhling, "Wide-field tcspc: methods and applications," *Measurement Science and Technology*, vol. 28, no. 1, p. 012003, 2016.

[18] S. Trautmann, V. Buschmann, S. Orthaus, F. Koberling, U. Ortmann, and R. Erdmann, "Fluorescence lifetime imaging (flim) in confocal microscopy applications: an overview," *PicoQuant GmbH*, vol. 29, p. 12489, 2013.

[19] W. Becker, A. Bergmann, and C. Biskup, "Multispectral fluorescence lifetime imaging by tcspc," *Microscopy research and technique*, vol. 70, no. 5, pp. 403–409, 2007.

[20] N. Förster, "Fluorescence lifetime imaging for chemical sensing," 2020.

[21] J. McGinty, J. Requejo-Isidro, I. Munro, C. Talbot, P. Kellett, J. Hares, C. Dunsby, M. Neil, and P. French, "Signal-to-noise characterization of time-gated intensifiers used for wide-field time-domain flim," *Journal of Physics D: Applied Physics*, vol. 42, no. 13, p. 135103, 2009.

[22] K. Greger, J. Swoger, and E. Stelzer, "Basic building units and properties of a fluorescence single plane illumination microscope," *Review of Scientific Instruments*, vol. 78, no. 2, p. 023705, 2007.

[23] J. G. Ritter, R. Veith, J.-P. Siebrasse, and U. Kubitscheck, "High-contrast single-particle tracking by selective focal plane illumination microscopy," *Optics express*, vol. 16, no. 10, pp. 7142–7152, 2008.

[24] O. E. Olarte, J. Andilla, E. J. Gualda, and P. Loza-Alvarez, "Light-sheet microscopy: a tutorial," *Advances in Optics and Photonics*, vol. 10, no. 1, pp. 111–179, 2018.

[25] P. A. Santi, "Light sheet fluorescence microscopy: a review," *Journal of Histochemistry & Cytochemistry*, vol. 59, no. 2, pp. 129–138, 2011.

[26] J. Palero, S. I. Santos, D. Artigas, and P. Loza-Alvarez, "A simple scanless two-photon fluorescence microscope using selective plane illumination," *Optics express*, vol. 18, no. 8, pp. 8491–8498, 2010.

[27] R. Li, A. Liu, T. Wu, W. Xiao, L. Tang, and L. Chen, "Digital scanned laser light-sheet fluorescence lifetime microscopy with wide-field time-gated imaging," *Journal of microscopy*, vol. 279, no. 1, pp. 69–76, 2020.

[28] A. Sherrard, P. Bishop, M. Panagi, M. B. Villagomez, D. Alibhai, and A. Kaidi, "Streamlined histone-based fluorescence lifetime imaging microscopy (flim) for studying chromatin organisation," *Biology open*, vol. 7, no. 3, p. bio031476, 2018.

[29] S. F. Silva, J. P. Domingues, and A. M. Morgado, "Accurate rapid lifetime determination on time-gated flim microscopy with optical sectioning," *Journal of healthcare engineering*, vol. 2018, 2018.

[30] B. Heeg, "Precision of mono-exponential decay estimates from rapid lifetime determination in the presence of signal photon and background noise," *Measurement Science and Technology*, vol. 25, no. 10, p. 105201, 2014.

[31] A. J. Walsh, R. S. Cook, M. E. Sanders, L. Aurisicchio, G. Ciliberto, C. L. Arteaga, and M. C. Skala, "Quantitative optical imaging of primary tumor organoid metabolism predicts drug response in breast cancer," *Cancer research*, vol. 74, no. 18, pp. 5184–5194, 2014.

[32] M. M. Lukina, V. V. Dudenkova, N. I. Ignatova, I. N. Druzhkova, S. Lyubov'E, E. V. Zagaynova, and M. V. Shirmanova, "Metabolic cofactors nad (p) h and fad as potential indicators of cancer cell response to chemotherapy with paclitaxel," *Biochimica et Biophysica Acta (BBA)-General Subjects*, vol. 1862, no. 8, pp. 1693–1700, 2018.

[33] W. Becker, A. Bergmann, R. S. Ibarrola, P.-F. Müller, and L. Braun, "Metabolic imaging by simultaneous flim of nad (p) h and fad," in *Multiphoton Microscopy in the Biomedical Sciences XIX*, vol. 10882, pp. 34–41, SPIE, 2019.

[34] M. Y. Berezin and S. Achilefu, "Fluorescence lifetime measurements and biological imaging," *Chemical reviews*, vol. 110, no. 5, pp. 2641–2684, 2010.

[35] P. GmbH, *"Picosecond Laser Diode Heads for PDL 800-D / PDL 828"*. PicoQuant GmbH, 2022.

[36] LaVision, *"PicoStar HR manual"*. LaVision, 2003.

[37] LaVision, *"Product-Manual DaVis 7.2 Software"*. LaVision, 2007.

[38] accessed: 09.2022, "https://www.edmundoptics.com/knowledge-center/application-notes/lasers/considerations-when-using-cylinder-lenses/."

[39] J. Huisken and D. Y. Stainier, "Selective plane illumination microscopy techniques in developmental biology," 2009.

[40] R. N. Hotchkiss, F. E. Washer, and F. W. Rosberry, "Spurious resolution of photographic lenses," *JOSA*, vol. 41, no. 9, pp. 600–603, 1951.

[41] S. Ram, E. S. Ward, and R. J. Ober, "Beyond rayleigh's criterion: a resolution measure with application to single-molecule microscopy," *Proceedings of the National Academy of Sciences*, vol. 103, no. 12, pp. 4457–4462, 2006.

[42] accessed: 09.2022, "https://www.olympus-lifescience.com/en/microscope-resource/primer/techniques/confocal/resolutionintro/."

[43] M. W. D. Kenneth R. Spring, Thomas J. Fellers, "Resolution and contrast in confocal microscopy."

[44] T. Funane, S. S. Hou, K. M. Zoltowska, S. J. van Veluw, O. Berezovska, A. T. Kumar, and B. J. Bacskai, "Selective plane illumination microscopy (spim) with time-domain fluorescence lifetime imaging microscopy (flim) for volumetric measurement of cleared mouse brain samples," *Review of Scientific Instruments*, vol. 89, no. 5, p. 053705, 2018.

[45] F. Lanni, B. Bailey, D. L. Farkas, and D. L. Taylor, "Excitation field synthesis as a means for obtaining enhanced axial resolution in fluorescence microscopes," *Bioimaging*, vol. 1, no. 4, pp. 187–196, 1993.

[46] A. Batista, "Two-photon imaging of the cornea using femtosecond laser microscopes and tomographs," 2018.

[47] P. Drössler, W. Holzer, A. Penzkofer, and P. Hegemann, "ph dependence of the absorption and emission behaviour of riboflavin in aqueous solution," *Chemical Physics*, vol. 282, no. 3, pp. 429–439, 2002.

[48] A. Batista, C. Loureiro, J. P. Domingues, J. S. Silva, and M. Morgado, "Flim as a tool for metabolic imaging of the cornea," in *2012 IEEE 2nd Portuguese Meeting in Bioengineering (ENBENG)*, pp. 1–4, IEEE, 2012.

[49] E. Instruments, "Fluorescence lifetime standards data table."

[50] A. Batista, H. G. Breunig, A. Uchugonova, A. M. Morgado, and K. König, "Two-photon spectral fluorescence lifetime and second-harmonic generation imaging of the porcine cornea with a 12-femtosecond laser microscope," *Journal of biomedical optics*, vol. 21, no. 3, p. 036002, 2016.

[51] S. Al-Fahdawi, R. Qahwaji, A. S. Al-Waisy, and S. Ipsopn, "An automatic corneal subbasal nerve registration system using fft and phase correlation techniques for an accurate dpn diagnosis," in *2015 IEEE International Conference on Computer and Information Technology; Ubiquitous Computing and Communications; Dependable, Autonomic and Secure Computing; Pervasive Intelligence and Computing*, pp. 1035–1041, IEEE, 2015.

Appendices

A

Appendix A

A.1 Data analysis

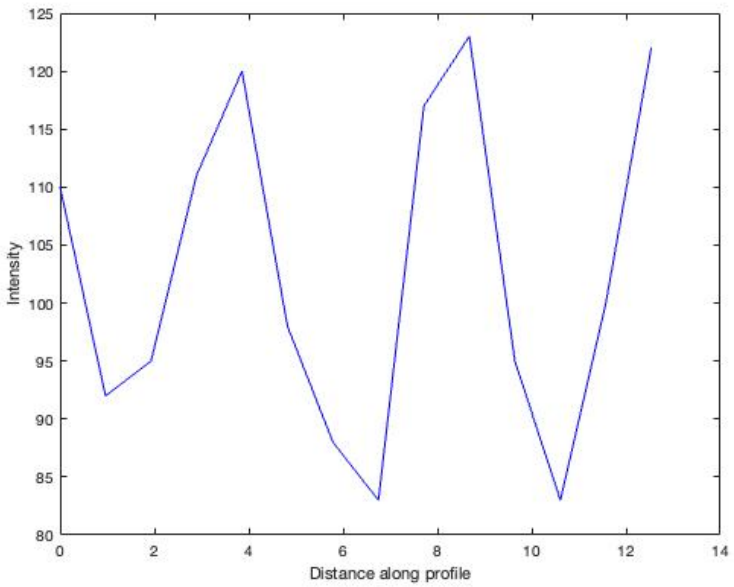

Figure A.1: Plot of the intensity data along x-axis pixels, corresponding to a perpendicular line over target test element 2 of group 7.

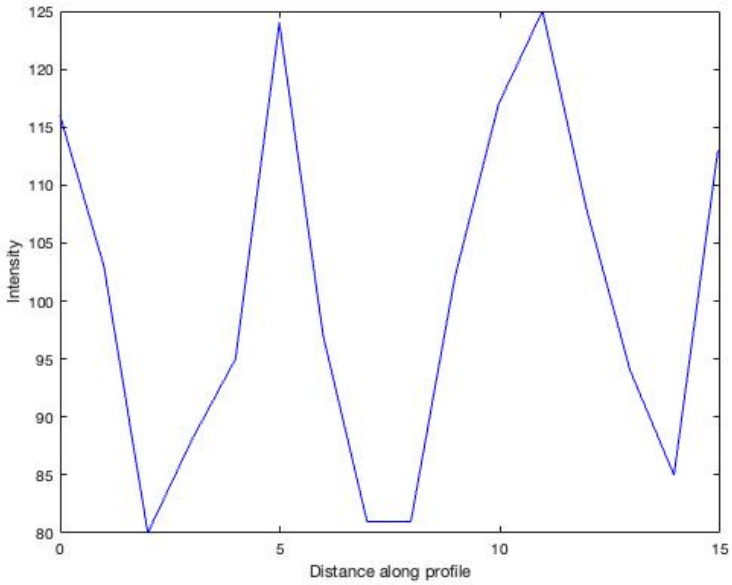

Figure A.2: Plot of the intensity data along y-axis pixels, corresponding to a perpendicular line over target test element 1 of group 7.

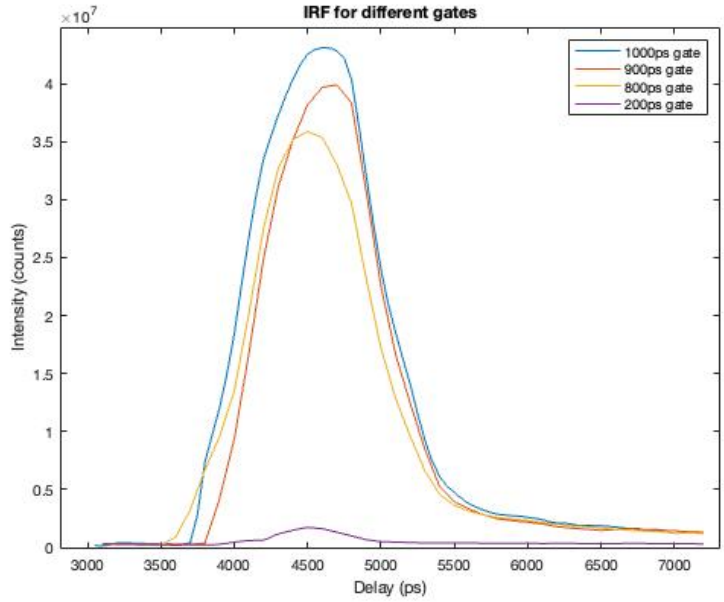

Figure A.3: Measured IRF for gates widths of 1000, 900, 800, and 200 ps.